Large Eddy Simulation for the Streamfunction Formulation of the Quasigeostrophic Equations of the Ocean

Erich L Foster

Thesis proposal for

Doctor of Philosophy
in
Mathematics

Traian Iliescu, Chair
Slimane Adjerid
John A. Burns
Anne Staples

02 May 2012
Blacksburg, Virginia

Keywords: Quasigeostrophic equations, finite element method, Argyris element.

Large Eddy Simulation for the Streamfunction Formulation of the Quasigeostrophic Equations of the Ocean

Erich L Foster

(ABSTRACT)

We present a Large Eddy Simulation model of the conforming finite element discretization of the streamfunction formulation of the one-layer quasigeostrophic equations, which are a commonly used model for the large scale wind-driven ocean circulation. Optimal error estimates for this finite element discretization with the Argyris element and for the large eddy simulation will be derived. Numerical tests for the finite element discretization and large eddy simulation of the quasigeostrophic equations. Additionally, numerical tests for two of its standard simplifications (the linear Stommel model and the linear Stommel-Munk model) are carried out. By benchmarking the numerical results against those in the published literature, we conclude that our finite element discretization is accurate. Furthermore, the numerical results have the same convergence rates as those predicted by the theoretical error estimates.

Contents

1 Introduction **1**
- 1.1 Motivation . . . 1
- 1.2 Problem Overview . . . 2
- 1.3 Existing Research . . . 4
- 1.4 Proposal Outline . . . 5

2 Governing Equations **6**
- 2.1 The Quasi-Geostrophic Equations . . . 6
- 2.2 Stationary QGE . . . 10
- 2.3 Large Eddy Simulation . . . 11

3 Weak Solutions and Well Posedness **12**
- 3.1 QGE Weak Formulation . . . 12
- 3.2 SQGE Weak Formulation . . . 14
  - 3.2.1 Well-Posedness of SQGE . . . 14
- 3.3 LES Weak Formulation . . . 15

4 Finite Element Formulation **16**
- 4.1 QGE Finite Element Formulation . . . 16
- 4.2 SQGE Finite Element Formulation . . . 16
- 4.3 LES Finite Element Formulation . . . 17
- 4.4 Argyris Element . . . 18
  - 4.4.1 Basis Functions . . . 19
  - 4.4.2 Transformation . . . 22
  - 4.4.3 Normal Derivatives . . . 27
  - 4.4.4 Interpolation Error . . . 28
- 4.5 Two Level Method . . . 28
  - 4.5.1 Two Level Algorithm . . . 29
- 4.6 Method of Lines . . . 30

5 Error Analysis **31**
- 5.1 SQGE . . . 31
  - 5.1.1 Two Level Method . . . 36
- 5.2 QGE . . . 38
- 5.3 LES . . . 38

6 Numerical Tests **39**
6.1 SQGE . . . 39
6.1.1 Linear Stommel Model . . . 40
6.1.2 Linear Stommel-Munk Model . . . 43
6.1.3 Stationary Quasigeostrophic Equations . . . 45
6.2 SQGE Two-Level . . . 47
6.3 QGE . . . 49
6.4 LES . . . 49

7 Future Work **50**

Bibliography **51**

List of Tables

4.1 Constraints for Argyris triangle 20
4.2 Coefficients for the Argyris Basis Matrix, M 21

6.1 Errors and Rate of Convergence for the Linear Stommel Model (6.5), Test 1 [48] . . 41
6.2 Errors and Rate of Convergence for the Linear Stommel Model (6.5), Test 1b [48] . . 42
6.3 Errors and Rate of Convergence for the Linear Stommel Model (6.5), Test 2 [39] . . 43
6.4 Errors and Rate of Convergence for the Linear Stommel-Munk Model (6.8), Test 3 [6] 44
6.5 Errors and Rate of Convergence for the Linear Stommel-Munk Model (6.8), Test 4 [6] 45
6.6 Errors and Rate of Convergence for the Full SQGE (2.28), Test 5 46
6.7 Errors and Rate of Convergence for the Full SQGE (2.28), Test 6 47
6.8 Benchmark Errors and Rate of Convergence SQGE (2.28). 48
6.9 Errors and Rate of Convergence in h for the Two-Level method applied to SQGE (2.28). 48
6.10 Errors and Rate of Convergence in H for the Two-Level method applied to SQGE (2.28). 49

7.1 Steps to finish thesis and proposed timeline. 50

List of Figures

1.1 Map of the Gulf Stream by Franklin-Folger, 1769 1
1.2 Ocean Surface Currents 2

4.1 Argyris element with its 21 degrees of freedom. 18
4.2 The reference triangle $\widehat{K}$ for Argyris 19
4.3 Demonstration of Continuity Issue in Normal Derivatives 28

6.1 Linear Stommel Model (6.5), Test 1a [48]: Streamlines of the approximation, ψ^h, $h = \frac{1}{32}$, and 9670 DoFs. 41
6.2 Linear Stommel Model (6.5), Test 1b [48]: Streamlines of the approximation, ψ^h, $h = \frac{1}{32}$, and 9670 DoFs with $\epsilon_s = 1$. 42
6.3 Linear Stommel Model (6.5), Test 2 [39]: Streamlines of the approximation, ψ^h, $h = \frac{1}{32}$, and 9670 DoFs. 43
6.4 Linear Stommel-Munk Model (6.8), Test 3 [6]: Streamlines of the approximation, ψ^h, on a mesh size, $h = \frac{1}{32}$, and 28550 DoFs. 44
6.5 Linear Stommel-Munk Model (6.8), Test 4 [6]: Streamlines of the approximation, ψ^h, $h = \frac{1}{32}$, and 28550 DoFs. 45
6.6 Full SQGE (2.28), Test 5: Streamlines of the approximation, ψ^h, $h = \frac{1}{32}$, and 28550 DoFs. 46
6.7 Full SQGE (2.28), Test 6: Streamlines of the approximation, ψ^h, $h = \frac{1}{32}$, and 28550 DoFs. 47

Chapter 1

Introduction

1.1 Motivation

Ocean currents have influenced humanity since the beginning of time, both through the effects ocean currents have on climate, but also through the effects they have on human travel. Vikings and Polynesians both made use of ocean currents in their exploration [13, 27]. The Vikings used the ocean currents to travel between Europe and the Americas [27]. In fact, the Vikings were able to sail all along the Greenland coast, because of a lack of ice bergs caused by a more northerly reaching Gulf Stream, which receded a century later [38].

The first documentation of ocean currents were made by Christopher Columbus (1492-1494), Vasco da Gama (1497-1499), and Ferdinand Magellan (1519-1522). In fact, the Gulf Stream was first mapped by Benjamin Franklin in 1769 (Figure 1.1) [13, 48]. The first instrumental observations of ocean currents on a global scale were begun by the HMS *Challenger* in 1872 when she set sail for over three years around the world [46].

Figure 1.1: Map of the Gulf Stream by Franklin-Folger, 1769

In more recent times we read of plans for shipping through the Northwestern Passage, which until recently had been closed by sea ice. Numerical climate models predicted that the passage would eventually open, however the passage has opened much earlier than anticipated [42]. Canada claims it has full rights to the passage while the United States and Europe claim it is part of international waters. On the other hand Russia has laid claims to the sea floor in the artic and thereby raising

tensions in the region. Clearly, climate change can influence geopolitics.

The climate system is driven by energy from the sun. This solar energy is transfered from the low latitudes to the high latitudes via radiative processes, and oceanic and atmosphic circulations. The oceans make up approximately 71% of the Earths surface, therefore the absorption of solar energy is dominated by the oceans. Thus, climate variability is, to a large extent, an ocean-related phenomenon [46]. Because of this we see that ocean circulation changes are strongly linked to changes in climate [38, 46]. In fact, the cold periods in Western Europe during the time periods 1440-1460, 1687-1703, and 1808-1821 can all be linked to a southward deflection of the Gulf Stream and a southward penetration of Arctic cold water [38].

The large scale ocean flows are characterized by three major features: the wind forcing, stratification, and the effects of rotation [34, 48]. Annual mean wind patterns, where winds are westerward near the equator and eastward at the midlatitudes [13], drive the subtropical and subpolar gyres, which correspond to the strong, persistent, sub-tropical and sub-polar western boundary currents: in the North Atlantic (the Gulf Stream and the Labrador Current), in the South Atlantic (the Brazil and the Falkland Currents), in North Pacific (the Kuroshio and the Oyashio Currents), in the South Pacific (East Australia Current) and in the Indian Ocean (the Agulhas Current) [13, 48]. These major ocean currents are dipicted in Figure 1.2. One of the common features of these gyres is that they display strong western boundary currents, weaker interior flows, and weak eastern boundary currents. Its these wind-driven ocean circulations that play a significant role in climate dynamics [12, 19].

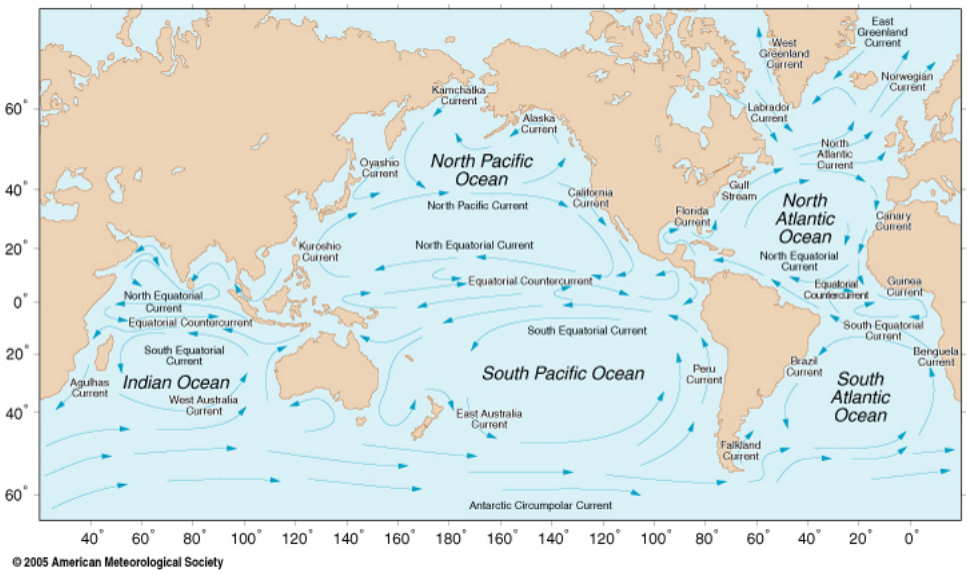

Figure 1.2: Ocean Surface Currents

1.2 Problem Overview

With the continuous increase in computational power, complex mathematical models are becoming more and more popular in the numerical simulation of oceanic and atmospheric flows. For some geophysical flows in which computational efficiency is of paramount importance, however, simplified mathematical models are central. For example, the *quasi-geostrophic equations (QGE)*, a standard mathematical model for large scale oceanic and atmospheric flows [11, 34, 41, 48], are often used

in climate modeling [12].

The QGE are usually discretized in space by using the *finite difference method* (FDM) [43]. The *finite element method* (FEM), however, offers several advantages over the popular FDM, as outlined in [39]: (i) an easy treatment of complex boundaries, such as those of continents for the ocean, or mountains for the atmosphere; (ii) an easy grid refinement to achieve a high resolution in regions of interest [6]; (iii) a natural treatment of boundary conditions; and (iv) a straightforward approach for the treatment of multiply connected domains [39]. Despite these advantages, there are relatively few papers that consider the FEM applied to the QGE [6, 17, 32, 39, 47].

To our knowledge, *all* the FEM discretizations of the QGE have been developed for the streamfunction-vorticity formulation, none using the streamfunction formulation. The reason is simple: The streamfunction-vorticity formulation yields a second order *partial differential equation (PDE)*, whereas the streamfunction formulation yields a fourth order PDE. Thus, although the streamfunction-vorticity formulation has two variables (q and ψ) and the streamfunction formulation has just one (ψ), the former is the preferred formulation used in practical computations, since its conforming FEM discretization requires low-order (C^0) elements, whereas the latter requires high-order (C^1) elements.

The streamfunction formulation is, from both mathematical and computational points of view, completely different from the vorticity-streamfunction formulation. Indeed, the FEM discretization of the streamfunction formulation generally requires the use of C^1 elements (for a conforming discretization), which makes their implementation challenging. From a mathematical point of view, however, the streamfunction formulation has the following significant advantage over the vorticity-streamfunction formulation: there are optimal error estimates for the FEM discretization of the streamfunction formulation (see the error estimate (13.5) and Table 13.1 in [23]), whereas the available error estimates for the vorticity-streamfunction formulation are suboptimal.

Despite the simplification made in formulating the QGE from the full-fledged equations of ocean, the numerical simulation of the QGE is still computationally challenging when integrating over long time periods, as is the case in climate modeling. Therefore, it is necessary to reduce the computational cost of QGE simulations. We will consider two (not necessarily independent) approaches to reducing this computational cost; The first, by using a *Two-Level* method to calculate the streamfunction at each time step, and the second approach will be to apply *Large Eddy Simulation (LES)*, namely *Approximate Deconvolution* (AD), to the QGE. To our knowledge it will be the first time either of these approaches have been applied to the streamfunction formulation of the QGE.

Two-level finite element discretizations are very promising approaches for finite element discretizations of nonlinear partial differential equations [15, 30]. A Two-level finite element discretizations aims to solve a particular nonlinear elliptic equation by first solving the system on a coarse mesh and then using the coarse mesh solution as a linearized variable to solve the linearized elliptic equation on a fine mesh. The attraction of such a method is that one need only solve the nonlinear equations on a coarse mesh and then use this solution to solve on a fine mesh, thereby reducing computational time without sacrificing much in the way of solution accuracy. The development of the two-level finite element discretization was originally by Xu in [51] and later algorithms for the Navier-Stokes Equations (NSE) were developed by Layton [30], Fairag [15, 16], and Shao [45].

LES was developed mainly by the engineering and geophysics communities and has emerged as one of the most promising approaches for modeling turbulent flows [26]. In LES only the large spatial structures are computed directly while the interaction with small scales are modeled, allowing for a coarser spatial mesh. This coarser mesh leads to lower computational cost as compared to the *direct numerical simulation* (DNS). However, when using LES one must address the *closure*

problem. This closure problem is essentially the relationship between the energy cascade from small scales to large scales, in two dimensional flows, or from large scales to small scales, in three dimensional flows. Most of the development for LES models have been for 3D engineering flows [4]. Due to the difference in the energy cascade for 3D (forward energy cascade), as compared to 2D flows (inverse energy cascade), these LES closure models aren't appropriate for geophysical flows [43].

The goals of this paper are five-fold. First, we use a C^1 finite element (the Argyris element) to discretize the streamfunction formulation of the QGE. To the best of our knowledge, this is the *first* time that a C^1 finite element has been used in the numerical discretization of the QGE. Second, we derive optimal error estimates for the FEM discretization of the QGE and present supporting numerical experiments. To the best of our knowledge, this is the *first* time that optimal error estimates for the QGE have been derived. Third, we present a Two-Level algorithm for solving the streamfunction formulation of the QGE and present the error analysis associated with this algorithm. To the best of our knowledge, this is the *first* time that such an algorithm has been applied the the streamfunction formulation of the QGE. Fourth, we will present an LES closure model for the streamfunction formulation of the QGE and its theoretical framework. To the best of our knowledge, this is the *first* time that LES has been applied to the streamfunction formulation of the QGE. Finally, we will present a finite element error analysis associated with the LES closure model applied to the streamfunction formulation of the QGE. To the best of our knowledge, this is the *first* time that such an error analysis has been derived for LES applied to the streamfunction formulation of the QGE.

1.3 Existing Research

Although the FEM discretization of the QGE is relatively scarce, the corresponding error analysis seems to be even more scarce. To our knowledge, *all* the error analysis for the FEM discretization of the QGE has been done for the vorticity-streamfunction formulation, none being done for the streamfunction formulation. Furthermore, to the best of our knowledge, all the available error estimates for the FEM discretization of the QGE are *suboptimal*. The first FEM error analysis for the FEM discretization of the QGE was carried out by Fix [17], in which suboptimal error estimates for the vorticity-streamfunction formulation were proved. Indeed, relationships (4.7) and (4.8) (and the discussion above these) in [17] show that the FEM approximations for *both* the potential vorticity (denoted by ζ) and streamfunction (denoted by ψ) consist of piecewise polynomials of degree $k-1$. At the top of page 381, the author concludes that the error analysis yields the following estimates:

$$\|\psi - \psi^h\|_1 = O(h^{k-1}), \tag{1.1}$$
$$\|\zeta - \zeta^h\|_0 = O(h^{k-1}). \tag{1.2}$$

Although the streamfunction error estimate (1.1) appears to be optimal, the potential vorticity error estimate (1.2) is clearly suboptimal. Indeed, using piecewise polynomials of degree $k-1$ for the FEM approximation of the vorticity, one would expect an $O(h^k)$ error estimate in the L^2 norm. Medjo [36, 37] used a FEM discretization of the vorticity-streamfunction formulation and proved error estimates for the time discretization, but no error estimates for the spatial discretization. Finally, Cascon et al. [6] proved both *a priori* and *a posteriori* error estimates for the FEM discretization of the *linear Stommel-Munk* model (see Section 6 for more details). This model, while similar to the QGE, has one significant difference: the linear Stommel-Munk model is linear, whereas the QGE is nonlinear.

We note that the state-of-the-art in the FEM error analysis for the QGE seems to reflect that for the *two-dimensional Navier-Stokes equations (2D NSE)*, to which the QGE are similar in form. Indeed, as carefully discussed in [23], the 2D NSE in streamfunction-vorticity formulation are easy to implement (only C^0 elements are needed for a conforming discretization), but the available error estimates are suboptimal (see Section 11.6 in [23]). Next, we summarize the discussion in [23], since we believe it sheds light on the QGE setting. For C^0 piecewise polynomial of degree k FEM approximation for *both* the vorticity (denoted by ω) and streamfunction (denoted by ψ), the error estimates given in [21] are (see (1.26) in [23]):

$$|\psi - \psi^h|_1 + \|\omega - \omega^h\|_0 \leq C\, h^{k-1/2}\, |\ln h|^\sigma, \tag{1.3}$$

where $\sigma = 1$ for $k = 1$ and $\sigma = 0$ for $k > 1$. It is noted in [23] that the error estimate in (1.3) is not optimal: one may loose a half power in h for the derivatives of the streamfunction (i. e., for the velocity), and three-halves power for the vorticity. It is also noted that there is computational and theoretical evidence that (1.3) is not sharp with respect to the streamfunction error. Furthermore, in [18] it was shown that, for the *linear* Stokes equations, the derivatives of the streamfunction are essentially optimally approximated (see (11.27) in [23]):

$$|\psi - \psi^h|_1 \leq C\, h^{k-\varepsilon}, \tag{1.4}$$

where $\varepsilon = 0$ for $k > 1$ and $\varepsilon > 0$ is arbitrary for $k = 1$. That being said, it is then noted in [23] that (1.3) seems to be sharp for the vorticity error and thus vorticity approximations are, in general, very poor.

There has been extensive research in the area of closure models for three dimensional engineering flows, however the same cannot be said for geophysical flows [4, 43]. In fact, to our knowledge LES has not been applied to the pure streamfunction formulation of the QGE using finite elements. In [43] they apply the AD method to streamfunction vorticity formulation of the QGE, but using a finite difference scheme rather than for a FE scheme. So here will be adding two aspects to their work. That is, we will add the LES applied to a pure streamfunction formulation of QGE with a FE discretization. Therefore, the biggest contribution of this thesis will be in this area.

1.4 Proposal Outline

The rest of the paper is organized as follows: Section 2.1 presents the QGE, Section 2.2 presents the stationary QGE, and Section 2.3 presents the filter QGE and a discussion on the appropriate closure model. Then Chapter 3 will discusses the well posedness of both the QGE and SQGE with special attention paid to the weak formulations and the mathematical support for the weak formulation presented in Section 3.1 and Section 3.2 for the QGE and SQGE, respectively. Additionally, the weak formulation of the filtered QGE are presented in Section 3.3. In Chapter 4 we outline the FEM discretization for the QGE (Section 4.1), SQGE (Section 4.2, and Filtered QGE (Section 4.3), with special emphasis placed on the Argyris element in Section 4.4. Additional, a discussion of the Two-Level method is presented in Section 4.5. Rigorous error estimates for the FE discretization and the Two-Level method applied to the stationary QGE are derived in Section 5.1 and Subsection 5.1.1, respectively. Several numerical experiments supporting the theoretical results for the SQGE and the Two-Level method are presented in Section 6.1 and Section 6.2. Finally, conclusions and our future research directions are included in Chapter 7.

Chapter 2

Governing Equations

2.1 The Quasi-Geostrophic Equations

One of the most popular mathematical models used in the study of large scale wind-driven ocean circulation is the QGE [11, 48]. The QGE represent a simplified model of the full-fledged equations (e.g., the Boussinesq equations), which allows efficient numerical simulations while preserving many of the essential features of the underlying large scale ocean flows. The assumptions used in the derivation of the QGE include the hydrostatic balance, the β-plane approximation, the geostrophic balance, and the eddy viscosity parametrization. Details of the derivation of the QGE and the approximations used along the way can be found in standard textbooks on geophysical fluid dynamics, such as [11, 34, 33, 35, 41, 48].

In the *one-layer QGE*, sometimes called the barotropic vorticity equation, the flow is assumed to be homogenous in the vertical direction. Thus, stratification effects are ignored in this model. The practical advantages of such a choice are obvious: the computations are two-dimensional, and, thus, the corresponding numerical simulation have a low computational cost. To include stratification effects, QGE models of increasing complexity have been devised by increasing the number of layers in the model (e.g., the two-layer QGE and the N-layer QGE [48]). As a first step, in this report we use the one-layer QGE (referred to as "the QGE" in what follows) to study the wind-driven circulation in an enclosed, midlatitude rectangular basin, which is a standard problem, studied extensively by modelers [11, 31, 33, 34, 35, 48, 41].

The QGE are usually written as follows (see, e.g., equation (14.57) in [48], equation (1.1) in [34], equation (1.1) in [49], and equation (1) in [22]):

$$\frac{\partial q}{\partial t} + J(\psi, q) = A\,\Delta q + F \tag{2.1}$$

$$q = \Delta\psi + \beta\, y, \tag{2.2}$$

where q is the potential vorticity, ψ is the velocity streamfunction, β is the coefficient multiplying the y coordinate (which is oriented northward) in the β-plane approximation (2.4), F is the forcing, A is the eddy viscosity parametrization, and $J(\cdot,\cdot)$ is the Jacobian operator given by

$$J(\psi, q) := \frac{\partial \psi}{\partial x}\frac{\partial q}{\partial y} - \frac{\partial \psi}{\partial y}\frac{\partial q}{\partial x}. \tag{2.3}$$

The β-plane approximation reads

$$f = f_0 + \beta\, y, \tag{2.4}$$

where f is the Coriolis parameter and f_0 is the reference Coriolis parameter (see, e.g., the discussion on page 84 in [10] or Section 2.3.2 in [48]).

As noted in Chapter 10.7.2 in [48] (see also [44]), the eddy viscosity parameter A in (2.1) is usually several orders of magnitude higher than the molecular viscosity. This choice allows the use of a coarse mesh in numerical simulations. The horizontal velocity $\mathbf{u}$ can be recovered from ψ and q by using the following formula:

$$\mathbf{u} := \nabla^{\perp}\psi = \begin{pmatrix} -\frac{\partial \psi}{\partial y} \\ \frac{\partial \psi}{\partial x} \end{pmatrix}. \tag{2.5}$$

The computational domain is standard [22], a rectangular, closed basin on a β-plane with the y coordinate increasing northward and the x coordinate eastward. The center of the basin is at $y = 0$, the northern and southern boundaries are at $y = \pm L$, respectively, and the western and eastern boundaries are at $x = 0$ and $x = L$ (see Figure 1 in [22]).

We are now ready to nondimensionalize the QGE (2.1)-(2.2). There are several ways of nondimensionalizing the QGE, based on different scalings and involving different parameters (see standard textbooks, such as [11, 34, 41, 48]). Since the FEM error analysis in this report is based on a precise relationship among the nondimensional parameters of the QGE (see, e.g., (5.1)), we present below a careful nondimensionalization of the QGE.

We first need to choose a length scale and a velocity scale. The length scale we choose is L, the width of the computational domain. The velocity scale is the Sverdrup velocity

$$U := \frac{\pi\,\tau_0}{\rho\,H\,\beta\,L}, \tag{2.6}$$

where τ_0 is the amplitude of the wind stress, ρ is the density of the fluid, and H is the height of the fluid. The Sverdrup balance, which was used in the derivation of (2.6), expresses the balance between the two dominant effects in the system: the β-effect and the curl of the divergence of the wind stress (see, e.g., Section 14.1.3 in [48]). Once the length and velocity scales are chosen, the variables in the QGE (2.1)-(2.2) can be nondimensionalized as follows:

$$x^* = \frac{x}{L}, \quad y^* = \frac{y}{L}, \quad t^* = \frac{t}{L/U}, \quad q^* = \frac{q}{\beta\,L}, \quad \psi^* = \frac{\psi}{U\,L}, \tag{2.7}$$

where a * superscript denotes the nondimensional variable. We first nondimensionalize (2.2). Using (2.7), (2.2) becomes

$$\beta\,L\,q^* = \frac{1}{L^2}\,\Delta^*(U\,L\,\psi^*) + \beta\,(L\,y^*). \tag{2.8}$$

Dividing (2.8) by $\beta\,L$, we get:

$$q^* = \left(\frac{U}{\beta\,L^2}\right)\,\Delta^*\psi^* + y^*. \tag{2.9}$$

Defining the *Rossby number* Ro as follows

$$Ro := \frac{U}{\beta\,L^2}, \tag{2.10}$$

equation (2.9) becomes

$$q^* = Ro\,\Delta^*\psi^* + y^*. \tag{2.11}$$

We note that all the nondimensionalizations in (2.7) are naturally based on the velocity scale U and the length scale L, except q^*. Indeed, a nondimensionalization of the form

$$\widetilde{q} = \frac{U}{L}, \tag{2.12}$$

would probably be more natural. Note that the alternative nondimensionalization in (2.12) is indeed correct, i.e., the variable $\widetilde{q}$ is nondimensional. The main reason for which the nondimensionalization in (2.7) is used instead the one in (2.12) is that the former yields just one constant (the Rossby number Ro) in (2.11), whereas the latter would yield two constants.

Next, we nondimensionalize (2.1). We start with the left-hand side:

$$\frac{\partial q}{\partial t} = (\beta\, U)\, \frac{\partial q^*}{\partial t^*}, \tag{2.13}$$

$$\begin{aligned} J(\psi, q) &= \frac{\partial \psi}{\partial x}\,\frac{\partial q}{\partial y} - \frac{\partial \psi}{\partial y}\,\frac{\partial q}{\partial x} = U\,\frac{\partial \psi^*}{\partial x^*}\,\beta\,\frac{\partial q^*}{\partial y^*} - U\,\frac{\partial \psi^*}{\partial y^*}\,\beta\,\frac{\partial q^*}{\partial x^*} \\ &= (\beta\, U)\, J^*(\psi^*, q^*). \end{aligned} \tag{2.14}$$

Next, we nondimensionalize the right-hand side of (2.1). The first term can be nondimensionalized as follows:

$$\begin{aligned} \frac{\partial q}{\partial t} A\,\Delta q = A\left(\frac{\partial^2 q}{\partial x^2} + \frac{\partial^2 q}{\partial y^2}\right) &= A\left(\frac{1}{L^2}\,\frac{\partial^2}{\partial x^{*2}}\,(\beta\, L\, q^*) + \frac{1}{L^2}\,\frac{\partial^2}{\partial y^{*2}}\,(\beta\, L\, q^*)\right) \\ &= A\,\frac{\beta}{L}\,\Delta^* q^*. \end{aligned} \tag{2.15}$$

Thus, inserting (2.13)-(2.15) in (2.1), we get:

$$(\beta\, U)\,\frac{\partial q^*}{\partial t^*} + (\beta\, U)\, J^*(\psi^*, q^*) = A\,\frac{\beta}{L}\,\Delta^* q^* + F. \tag{2.16}$$

Dividing by $\beta\, U$, we get:

$$\frac{\partial q^*}{\partial t^*} + J^*(\psi^*, q^*) = \left(\frac{A}{U\, L}\right)\,\Delta^* q^* + \frac{F}{\beta\, U}. \tag{2.17}$$

Defining the *Reynolds number* Re as follows

$$Re := \frac{U\, L}{A}, \tag{2.18}$$

equation (2.17) becomes

$$\frac{\partial q^*}{\partial t^*} + J^*(\psi^*, q^*) = Re^{-1}\,\Delta^* q^* + \frac{F}{\beta\, U}. \tag{2.19}$$

As noted above, the Sverdrup balance expresses the balance between the two dominant effects in the system: the β-effect and the curl of the divergence of the wind stress (see, e.g., Section 14.1.3 in [48]). The velocity scale U in (2.6) was chosen according to the Sverdrup balance. Thus, the last term on the right-hand side of (2.19) has the following units:

$$\left[\frac{F}{\beta\, U}\right] \sim \left[\frac{\frac{\nabla\times(\nabla\cdot\tau_0)}{\rho}}{\beta\, U}\right] \overset{(2.6)}{\sim} \left[\frac{\frac{\nabla\times(\nabla\cdot\tau_0)}{\rho}}{\frac{\pi\,\tau_0}{\rho\, H\, L}}\right], \tag{2.20}$$

which, after the obvious simplification, is clearly nondimensional. Thus, (2.20) clearly shows that the last term on the right-hand side of (2.19) is nondimensional, so (2.19) becomes:

$$\frac{\partial q^*}{\partial t^*} + J^*(\psi^*, q^*) = Re^{-1}\,\Delta^* q^* + F^*. \tag{2.21}$$

Dropping the * superscript in (2.21), we obtain the nondimensional *vorticity-streamfunction formulation* of the *one-layer quasigeostrophic equations*

$$\frac{\partial q}{\partial t} + J(\psi, q) = Re^{-1}\,\Delta q + F \tag{2.22}$$

$$q = Ro\,\Delta\psi + y, \tag{2.23}$$

where Re and Ro are the Reynolds and Rossby numbers, respectively.

Substituting (2.23) in (2.22) and dividing by Ro, we get the *streamfunction formulation* of the *one-layer quasigeostrophic equations*

$$\frac{\partial\,[\Delta\psi]}{\partial t} - Re^{-1}\,\Delta^2\psi + J(\psi, \Delta\psi) + Ro^{-1}\,\frac{\partial\psi}{\partial x} = Ro^{-1}\,F. \tag{2.24}$$

Equations (2.22)-(2.23) and (2.24) are the usual formulations of the one-layer QGE in streamfunction-vorticity and streamfunction formulations, respectively. We note that the streamfunction-vorticity formulation has two unknowns (q and ψ), whereas the streamfunction formulation has only one unknown (ψ). The streamfunction-vorticity formulation, however, is more popular than the streamfunction formulation, since the former is a second-order PDE, whereas the latter is a fourth-order PDE.

We also note that (2.23)-(2.22) and (2.24) are similar in form to the 2D NSE written in the streamfunction-vorticity and streamfunction formulations, respectively. Indeed, (2.22)-(2.23) and (2.24) are almost the same as (11.3)-(11.4) and (13.1) in [23], which are obtained by first writing

$$\mathbf{u} = \begin{pmatrix} \frac{\partial\psi}{\partial y} \\ -\frac{\partial\psi}{\partial x} \end{pmatrix} \tag{2.25}$$

and then taking the curl of the 2D NSE.

There are, however, several significant differences between the QGE and the 2D NSE. First, we note that the term y in (2.23) and the corresponding term $\dfrac{\partial\psi}{\partial x}$ in (2.24), which model the *rotation effects* in the QGE, do not have counterparts in the 2D NSE. Furthermore, the Rossby number, Ro, in the QGE, which is a measure of the rotation effects, does not appear in the 2D NSE. However, apart from these two significant differences, the streamfunction-vorticity and streamfunction formulations of the QGE and the 2D NSE are quite similar.

Thus, for notation consistency (i.e., to ensure that the velocity and the streamfunction are related by (2.25)), we will consider the QGE (2.24) with ψ replaced with $-\psi$:

$$-\frac{\partial\,[\Delta\psi]}{\partial t} + Re^{-1}\,\Delta^2\psi + J(\psi, \Delta\psi) - Ro^{-1}\,\frac{\partial\psi}{\partial x} = Ro^{-1}\,F. \tag{2.26}$$

At this point, let us comment on the significance of the two parameters in (2.26), the Reynolds number Re and the Rossby number Ro. As in the 2D NSE case, Re is the coefficient of the diffusion term $-\Delta q = \Delta^2\psi$. The higher Re, the smaller the magnitude of the diffusion term as compared with the nonlinear convective term $-J(\psi, \Delta\psi) = (\nabla\psi^\perp \cdot \nabla)q = (\mathbf{u}\cdot\nabla)q$. Since Ro, quantifying

the rotation effects in the QGE, does not appear in the 2D NSE, its significance deserves a special attention. We first note that, for small Ro, which corresponds to large rotation effects, the forcing term $Ro^{-1} F$ becomes large as compared with the other terms. But probably the most interesting term in (2.26) is $Ro^{-1} \dfrac{\partial \psi}{\partial x}$, which could be interpreted as a convection type term with respect to ψ, not to $q = -\Delta\psi$. When Ro is small, $Ro^{-1} \dfrac{\partial \psi}{\partial x}$ becomes large. In conclusion, the physically relevant cases for large scale oceanic flows, in which Re is large and Ro is small (i.e., small diffusion and high rotation, respectively) translate mathematically into a *convection-dominated* PDE with *large forcing*. Thus, from a mathematical point of view, we expect the restrictive conditions used to prove the well-posedness of the 2D NSE [20, 21, 23] will be even more restrictive in the QGE setting, due to the rotation effects. We will later see that this is indeed the case.

To completely specify the equations in (2.26), we need to impose boundary conditions. The question of appropriate boundary conditions for the QGE is a thorny one, especially for the vorticity-streamfunction formulation (see [48, 9] for a careful discussion of this issue). In this report, we consider

$$\begin{aligned} \psi = \frac{\partial \psi}{\partial \mathbf{n}} = 0 \qquad & \text{on } \partial\Omega, \\ \psi = \psi_0 \qquad & \text{when } t = 0 \end{aligned} \tag{2.27}$$

which are also the boundary conditions used in [23] for the streamfunction formulation of the 2D NSE.

2.2 Stationary QGE

When testing Finite Element code it is useful to simplify the problem and so even though in the "real" world stationary "flows" don't exist the stationary QGE (SQGE) are useful in testing code. Additionally, the time dependence of the QGE ((2.24)) adds aditional complexity to the finite element error analysis. Finite error analysis for time dependent problems usualy can be split into two parts; analysis of the spatial discretization that arizes through the application of finite elements, and the discretization error in time that arizes from the application of the method of lines. Thus, a FE error analysis of the SQGE is a good push off point for analysis of the time-dependent QGE and is therefore the main motivation for presenting the SQGE.

The SQGE are obtained by setting $\dfrac{\partial q}{\partial t}$ to 0 in (2.22) and therefore we get the *streamfunction formulation* of the *one-layer stationary quasi-geostrophic equations*

$$Re^{-1}\,\Delta^2\psi + J(\psi, \Delta\psi) - Ro^{-1}\,\frac{\partial \psi}{\partial x} = Ro^{-1}\,F. \tag{2.28}$$

Equations (2.22)-(2.23), (2.24), and (2.28) are the usual formulations of the one-layer QGE in streamfunction-vorticity formulation, the one-layer QGE in streamfunction formulation, and the steady one-layer QGE in streamfunction formulation, respectively.

To completely specify the equations in (2.28), need to impose boundary conditions. For consistency and with the QGE ((2.24)) we consider

$$\psi = \frac{\partial \psi}{\partial \mathbf{n}} = 0 \qquad \text{on } \partial\Omega,$$

which, as stated previously, are also the boundary conditions used in [23] for the streamfunction formulation of the 2D NSE.

2.3 Large Eddy Simulation

In this section we discuss Large Eddy Simulation (LES). To our knowledge LES has not been applied to the finite element formulation of the streamfunction formulation of the QGE. It is the application of LES to this problem that will be the major contribution of this Thesis and therefore will be the main focus of the thesis.

To derive the quations for the filtered flow variable, $\overline{\psi}$, the QGE (2.26) has a spacial filter applied to it. Letting a bar denote the filtered variable, the filtered QGE reads:

$$-\frac{\partial[\Delta\overline{\psi}]}{\partial t} + Re^{-1}\Delta^2\overline{\psi} + J(\overline{\psi}, \Delta\overline{\psi}) - Ro^{-1}\frac{\partial\overline{\psi}}{\partial x} = Ro^{-1}\overline{F} + S \tag{2.29}$$

where S is the *subfilter-scale* term, given by

$$S = -\overline{J(\psi, \Delta\psi)} + J(\overline{\psi}, \Delta\overline{\psi}). \tag{2.30}$$

It is precisely this point where the closure model comes in, since the first term in the subfilter scale still requires the unfiltered variable. For the filtered QGE (2.29) to be closed the subfilter scale must be modeled in terms of the filtered variable $\overline{\psi}$, therefore closure models are necessary so as to close the filtered equation.

We propose to use *Approximate Deconvolution (AD)* for the closure model. The AD method uses repeated filtering in order to obtain an approximation to the unfiltered variable when the filtered variable is available. These approximations are used in the subfilter scale to close the model.

If we denote our spatial filtering operator by G then $G\psi = \overline{\psi}$. Using the fact that $G = I-(I-G)$ we can write the inverse filter G^{-1} using the Neumann series:

$$G^{-1} \approx \sum_{i=0}^{\infty}(I - G)^i. \tag{2.31}$$

For practical use we must truncate this series, thus truncating the series after N terms gives the approximate deconvolution operator, Q_N. Therefore the approximate deconvolution of ψ is obtained by

$$\psi \approx \psi^* = Q_N\overline{\psi}. \tag{2.32}$$

By increasing the value of N we get a more accurate approximation to the variable ψ. Using this idea of approximate convolution we can now approximate the Jacobian:

$$\overline{J(\psi, \Delta\psi)} \approx \overline{J(\psi^*, \Delta\psi^*)}. \tag{2.33}$$

Thus, we can close the filtered QGE (2.29) and we get the AD model

$$-\frac{\partial[\Delta\overline{\psi}]}{\partial t} + Re^{-1}\Delta^2\overline{\psi} + J(\overline{\psi}, \Delta\overline{\psi}) - Ro^{-1}\frac{\partial\overline{\psi}}{\partial x} = Ro^{-1}\overline{F} + S^* \tag{2.34}$$

where S^* is the subfilter scale modeled by

$$S^* = -\overline{J(\psi^*, \Delta\psi^*)} + J(\overline{\psi}, \Delta\overline{\psi}). \tag{2.35}$$

In the rest of this section we will discuss the AD model theory at length, since it is of great importance to model results.

Chapter 3

Weak Solutions and Well Posedness

3.1 QGE Weak Formulation

We are now ready to derive the weak formulation of the QGE in streamfunction formulation (2.26). To this end, it is necessary to introduce the appropriate functional setting. Here we will need to reference [5, 8, 6, 25, 24, 23, 31, 20, 20, 36] However, in light of the research still needed to be done to determine the appropriate functional setting for the weak form of QGE we will for now let

$$X := L^\infty(0,T;L^2(\Omega)) \cap L^2(0,T;H_0^2(\Omega))$$

where

$$L^2(0,T;H_0^2(\Omega)) := \left\{ \psi(t,\mathbf{x}) : [0,T] \to H_0^2(\Omega) : \int_0^T \|\Delta\psi\|\, dt < \infty \right\}$$
$$L^\infty(0,T;L^2(\Omega)) := \left\{ \psi(t,\mathbf{x}) : [0,T] \to L^2(\Omega) : \operatorname{ess}\sup_{0<t<T} \|\psi\| < \infty \right\}.$$

The choice for this space will have to be verify using the previously referred to references.

Multiplying (2.26) by a test function $\chi \in X$ and using the divergence theorem, we get in a standard way

$$\int_\Omega \left(-\frac{\partial\,[\Delta\psi]}{\partial t} + Re^{-1}\Delta^2\psi + J(\psi,\Delta\psi) - Ro^{-1}\frac{\partial\psi}{\partial x} \right) \chi\, d\mathbf{x} = Ro^{-1}\int_\Omega F\,\chi\, d\mathbf{x}$$

and then transferring some of the derivatives from ψ to χ. But first, we need to rewrite the Jacobian term, from (2.26) in a more useful form

$$-\frac{\partial}{\partial t}\int_\Omega \Delta\psi\,\chi\, d\mathbf{x} + Re^{-1}\int_\Omega \Delta^2\psi\, d\mathbf{x} - \int_\Omega \left(\frac{\partial\,[\Delta\psi]}{\partial x}\cdot\frac{\partial\psi}{\partial y} - \frac{\partial\,[\Delta\psi]}{\partial y}\cdot\frac{\partial\psi}{\partial x} \right) \chi\, d\mathbf{x}$$
$$- Ro^{-1}\int_\Omega \frac{\partial\psi}{\partial x}\,\chi\, d\mathbf{x} = Ro^{-1}\int_\Omega F\,\chi\, d\mathbf{x}$$
$$-\frac{\partial}{\partial t}\int_\Omega \Delta\psi\,\chi\, d\mathbf{x} + Re^{-1}\int_\Omega \Delta^2\psi\, d\mathbf{x} - \int_\Omega \nabla\,[\Delta\psi]\cdot\nabla\times\psi\,\chi\, d\mathbf{x} - Ro^{-1}\int_\Omega \frac{\partial\psi}{\partial x}\,\chi\, d\mathbf{x} = Ro^{-1}\int_\Omega F\,\chi\, d\mathbf{x}$$

For the remaining portion of the weak formulation we shall deal with each summand individually

(from left to right) and so

$$\begin{aligned}-\frac{\partial}{\partial t}\int_\Omega \Delta\psi\,\chi\,d\mathbf{x} &= -\frac{\partial}{\partial t}\int_\Omega \nabla\left(\nabla\psi\,\chi\right) - \nabla\psi\cdot\nabla\chi\,d\mathbf{x}\\ &= -\frac{\partial}{\partial t}\int_{\partial\Omega} \cancelto{0}{\nabla\psi\,\chi\cdot\mathbf{n}\,dS} + \frac{\partial}{\partial t}\int_\Omega \nabla\psi\nabla\chi\,d\mathbf{x}\end{aligned}$$

the next summand gives

$$\begin{aligned}Re^{-1}\int_\Omega \Delta^2\psi\,\chi\,d\mathbf{x} &= Re^{-1}\int_\Omega \nabla\left[\nabla^3\psi\,\chi\right] + \nabla^3\psi\nabla\chi\,d\mathbf{x}\\ &= Re^{-1}\int_{\partial\Omega} \cancelto{0}{\nabla^3\psi\,\chi\cdot\mathbf{n}\,dS} - Re^{-1}\int_\Omega \nabla\left[\Delta\psi\nabla\chi\right] - \Delta\psi\Delta\chi\,d\mathbf{x}\\ &= -Re^{-1}\int_{\partial\Omega} \cancelto{0}{\Delta\psi\nabla\chi\cdot\mathbf{n}\,dS} + Re^{-1}\int_\Omega \Delta\psi\Delta\chi\,d\mathbf{x}\end{aligned}$$

and the third and final summand that needs to be evaluated gives

$$\begin{aligned}-\int_\Omega \nabla\left[\Delta\psi\right]\cdot\nabla\times\psi\,\chi\,d\mathbf{x} &= -\int_\Omega \nabla\left[\Delta\psi\right]\cdot\nabla\times\psi\,\chi\,d\mathbf{x}\\ &= -\int_\Omega \nabla\left[\Delta\psi\cdot\nabla\times\psi\,\chi\right] - \Delta\psi\cdot\cancelto{0}{\nabla\left[\nabla\times\psi\chi\right]}\\ &\quad - \Delta\psi\cdot\nabla\times\psi\cdot\nabla\chi\,d\mathbf{x}\\ &= -\cancelto{0}{\int_{\partial\Omega}\Delta\psi\cdot\nabla\times\psi\,\chi\cdot\mathbf{n}\,dS}\\ &\quad + \int_\Omega \Delta\psi\cdot\nabla\times\psi\cdot\nabla\chi\,d\mathbf{x}\\ &= \int_\Omega \Delta\psi\left(\psi_y\chi_x - \psi_x\chi_y\right)\,d\mathbf{x}.\end{aligned}$$

Thus, the weak form of the QGE in streamfunction form is

$$\begin{aligned}\frac{\partial}{\partial t}\int_\Omega \nabla\psi\,\nabla\chi\,d\mathbf{x} + Re^{-1}\int_\Omega \Delta\psi\,\Delta\chi\,d\mathbf{x} + \int_\Omega \Delta\zeta\,\left(\psi_y\,\chi_x - \psi_x\,\chi_y\right)\,d\mathbf{x} - Ro^{-1}\int_\Omega \psi_x\,\chi\,d\mathbf{x}\\ = Ro^{-1}\int_\Omega F\,\chi\,d\mathbf{x} \qquad \forall\,\chi\in X.\end{aligned} \tag{3.1}$$

Therefore, letting

$$a_0(\psi,\chi) = \int_\Omega \nabla\psi\nabla\chi\,d\mathbf{x} \tag{3.2}$$

$$a_1(\psi,\chi) = Re^{-1}\int_\Omega \Delta\psi\,\Delta\chi\,d\mathbf{x}, \tag{3.3}$$

$$a_2(\zeta;\psi,\chi) = \int_\Omega \Delta\zeta\,\left(\psi_y\,\chi_x - \psi_x\,\chi_y\right)\,d\mathbf{x}, \tag{3.4}$$

$$a_3(\psi,\chi) = -Ro^{-1}\int_\Omega \psi_x\,\chi\,d\mathbf{x}, \tag{3.5}$$

$$\ell(\chi) = Ro^{-1}\int_\Omega F\,\chi\,d\mathbf{x}, \tag{3.6}$$

gives the following weak formulation of the QGE in streamfunction formulation:

$$\begin{gathered}\text{Find } \psi \in X \text{ such that} \\ \frac{\partial}{\partial t}a_0(\psi,\chi) + a_1(\psi,\chi)+a_2(\psi,\psi,\chi) + a_3(\psi,\chi) = \ell(\chi), \quad \forall \chi \in X.\end{gathered} \tag{3.7}$$

The linear form ℓ, the bilinear forms a_0, a_1, a_3 and the trilinear form a_2 are continuous [7]: There exists $\Gamma_1 > 0$ such that

$$|a_0(\psi,\chi)| \leq |\psi|_2 |\chi|_2 \quad \forall\, \psi,\chi \in X, \tag{3.8}$$
$$|a_1(\psi,\chi)| \leq Re^{-1}\, |\psi|_2\, |\chi|_2 \quad \forall\, \psi,\chi \in X, \tag{3.9}$$
$$|a_2(\zeta,\psi,\chi)| \leq \Gamma_1\, |\zeta|_2\, |\psi|_2\, |\chi|_2 \quad \forall\, \zeta,\psi,\chi \in X, \tag{3.10}$$
$$|a_3(\psi,\chi)| \leq Ro^{-1}\, |\psi|_2\, |\chi|_2 \quad \forall\, \psi,\, \chi \in X, \tag{3.11}$$
$$|\ell(\chi)| \leq Ro^{-1}\, \|F\|_{-2}\, |\chi|_2 \quad \forall\, \chi \in X. \tag{3.12}$$

3.2 SQGE Weak Formulation

We are now ready to derive the weak formulation of the SQGE in streamfunction formulation (2.28). To this end, we first introduce the appropriate functional setting. Let

$$X := H_0^2(\Omega) = \left\{ \psi \in H^2(\Omega) : \psi = \frac{\partial \psi}{\partial \mathbf{n}} = 0 \text{ on } \partial\Omega \right\}.$$

The difference in the functional setting for the QGE and the SQGE stems from the lack of time derivative in the SQGE. However, in the spacial domain everything remains the same.

Thus, the derivation of the weak formulation for the SQGE follows imediately from the weak formulation for the QGE with the exception that we set the bilinear form (3.2) to zero. Therefore, using the forms presented for the QGE weak form, i.e. (3.3), (3.4), (3.5), and (3.6), the weak form of the SQGE in streamfunction formulation is:

$$\begin{gathered}\text{Find } \psi \in X \text{ such that} \\ a_1(\psi,\chi) + a_2(\psi,\psi,\chi) + a_3(\psi,\chi) = \ell(\chi), \quad \forall \chi \in X.\end{gathered} \tag{3.13}$$

The linear form ℓ, the bilinear forms a_1, a_3 and the trilinear form a_2 are still continuous [7] and have the some bounds as those for the QGE, i.e. (3.9), (3.10), (3.11), and (3.12).

3.2.1 Well-Posedness of SQGE

For small enough data, one can use the same type of arguments as in [20, 21] to prove that the QGE in streamfunction formulation (3.13) are well-posed [2, 28, 50]. In what follows, we will always assume that the small data condition involving Re, Ro and F, is satisfied and, thus, that there exists a unique solution ψ to (3.13).

Using a standard argument (see Theorem 2.1 in [7]), one can also prove the following stability estimate:

Theorem 3.1. *The solution ψ of* (3.13) *satisfies the following stability estimate:*

$$|\psi|_2 \leq Re\, Ro^{-1}\, \|F\|_{-2}. \tag{3.14}$$

Proof. Setting $\chi = \psi$ in (3.13), we get:

$$a_1(\psi, \psi) + a_2(\psi, \psi, \psi) + a_3(\psi, \psi) = \ell(\psi). \tag{3.15}$$

Since the trilinear form a_2 is skew-symmetric in the last two arguments [20, 21, 23], we have

$$a_2(\psi, \psi, \psi) = 0. \tag{3.16}$$

We also note that, applying Green's theorem, we have

$$\begin{aligned} a_3(\psi, \psi) &= Ro^{-1} \iint_\Omega \frac{\partial \psi}{\partial x}\, dx\, dy \;=\; \frac{Ro^{-1}}{2} \iint_\Omega \frac{\partial}{\partial x}(\psi^2)\, dx\, dy \\ &= \frac{Ro^{-1}}{2} \iint_\Omega \left(\frac{\partial}{\partial x}(\psi^2) - \frac{\partial}{\partial x}(0) \right) dx\, dy \;=\; \frac{Ro^{-1}}{2} \int_{\partial\Omega} 0\, dx + \psi^2\, dy \\ &= 0, \end{aligned} \tag{3.17}$$

where in the last equality in (3.17) we used that $\psi = 0$ on $\partial\Omega$ (since $\psi \in H_0^2(\Omega)$). Substituting (3.17) and (3.16) in (3.15) and using the Cauchy-Schwarz inequality, we get:

$$\begin{aligned} a_1(\psi, \psi) &= \ell(\psi) \\ Re^{-1} \|\psi\|_2^2 &= Ro^{-1} (F, \psi) \qquad (3.18) \\ \|\psi\|_2 &\leq Re\, Ro^{-1} \sup_{\psi \in X} \frac{(F, \psi)}{|\psi|_2} \\ \|\psi\|_2 &\leq Re\, Ro^{-1} \|F\|_{-2}. \qquad (3.19) \end{aligned}$$

which proves (3.15). □

3.3 LES Weak Formulation

In this section the functional setting for the LES form of the QGE (2.24) will be presented. The weak formulation of the LES form of QGE will be different because LES requires a closure model. This extra term will show up in the weak formulation as an additional form. However, I don't believe the functional setting will change due to the extra term, but the extra term in the weak formulation will result in a different FE formulation presented in Section 4.3 and therefore a difference in the error analysis presented in Section 5.3.

Chapter 4

Finite Element Formulation

4.1 QGE Finite Element Formulation

In this section, we present the functional setting and some auxiliary results for the FEM discretization of the streamfunction formulation of the QGE (3.7). Let $\mathcal{T}^h$ denote a finite element triangulation of Ω with meshsize (maximum triangle diameter) h. We consider a *conforming* FEM discretization of (3.7), i.e., $X^h \subset X = H_0^2(\Omega)$.

The FEM discretization of the streamfunction formulation of the QGE (3.7) reads:

$$\begin{gathered} \text{Find } \psi^h \in X^h \text{ such that} \\ \frac{\partial}{\partial t} a_0(\psi^h, \chi^h) + a_1(\psi^h, \chi^h) + a_2(\psi^h, \psi^h, \chi^h) + a_3(\psi^h, \chi^h) = \ell(\chi^h), \quad \forall\, \chi^h \in X^h. \end{gathered} \tag{4.1}$$

Using standard arguments [20, 21], one can prove that, if the small data condition used in proving the well-posedness result for the continuous case holds, then (4.1) has a unique solution ψ^h (see Theorem 2.1 in [7]).

As noted in Section 6.1 in [8] (see also Section 13.2 in [23], Section 3.1 in [29], and Theorem 5.2 in [5], in order to develop a conforming FEM for the QGE (3.7), we are faced with the problem of constructing subspaces of the space $H_0^2(\Omega)$. Since the standard, piecewise polynomial FEM spaces are locally regular, this construction amounts in practice to finding FEM spaces X^h that satisfy the inclusion $X^h \subset C^1(\overline{\Omega})$, i.e., finding C^1 finite elements.

Several finite elements meet this requirement (see, e.g., Section 6.1 in [8], Section 13.2 in [23], and Section 5 in [5]): the Argyris triangular element, the Bell triangular element, the Hsieh-Clough-Tocher triangular element (a macroelement), and the Bogner-Fox-Schmit rectangular element).

A description of the particular finite element we are using (the Argyris triangle Figure 4.1) and its tranformation will be thouroughly discussed in Section 4.4). Additionaly, (4.1) is only a semi-discretization, since the formulation is still continuous in time, but discretized in space. Since there is no geometry in the time domain it makes sense to apply what has been called the *method of lines (MoL)* in the time domain, i.e. use a *finite difference* approximation for the time derivative. The MoL will be discussed further in Section 4.6.

4.2 SQGE Finite Element Formulation

In this section, we present the functional setting and some auxiliary results for the FEM discretization of the streamfunction formulation of the SQGE (3.13). Since the SQGE is QGE with

$\frac{\partial[\Delta\psi]}{\partial t} = 0$ the weak formulation is only different in that the derivative term does not exist. Thus, the functional space is simpler. Indeed, let $\mathcal{T}^h$ denote a finite element triangulation of Ω with meshsize (maximum triangle diameter) h. We consider a *conforming* FEM discretization of (3.13), i.e., $X^h \subset X = H_0^2(\Omega)$.

The FEM discretization of the streamfunction formulation of the SQGE (3.13) reads:

$$\begin{gathered}\text{Find } \psi^h \in X^h \text{ such that} \\ a_1(\psi^h, \chi^h) + a_2(\psi^h, \psi^h, \chi^h) + a_3(\psi^h, \chi^h) = \ell(\chi^h), \quad \forall\, \chi^h \in X^h.\end{gathered} \tag{4.2}$$

Using standard arguments [20, 21], one can prove that, if the small data condition used in proving the well-posedness result for the continuous case holds, then (4.2) has a unique solution ψ^h (see Theorem 2.1 in [7]). Furthermore, one can prove the following stability result for ψ^h using the same arguments as those used in the proof of (3.1) for the continuous setting.

Theorem 4.1. *The solution ψ^h of (4.2) satisfies the following stability estimate:*

$$|\psi^h|_2 \leq Re\, Ro^{-1} \|F\|_{-2}. \tag{4.3}$$

Proof. The proof is almost identical to the proof of Proposition 3.1, but is given here for completeness.

Let $\chi^h = \psi^h$ in (4.2) which gives

$$a_1(\psi^h, \psi^h) + a_2(\psi^h, \psi^h, \psi^h) + a_3(\psi^h, \psi^h) = \ell(\psi^h) \qquad \forall \pi^h \in X^h.$$

Since, $a_2(\psi^h, \psi^h, \psi^h) = 0$ and $a_3(\psi^h, \psi^h) = 0$ we have

$$\begin{aligned} a_1(\psi^h, \psi^h) &= \ell(\psi^h) \\ Re^{-1} \|\psi^h\|_2^2 &= Ro^{-1} (F, \psi^h) \\ \|\psi^h\|_2 &\leq Re\, Ro^{-1} \sup_{\psi^h \in X^h} \frac{(F, \psi^h)}{|\psi^h|_2} \\ \|\psi^h\|_2 &\leq Re\, Ro^{-1} \|F\|_{-2}. \end{aligned}$$

And the proof is complete. □

Again, we point out that as noted in Section 6.1 in [8] (see also Section 13.2 in [23], Section 3.1 in [29], and Theorem 5.2 in [5], in order to develop a conforming FEM for the SQGE (3.13), we are faced with the problem of constructing subspaces of the space $H_0^2(\Omega)$. Since the standard, piecewise polynomial FEM spaces are locally regular, this construction amounts in practice to finding FEM spaces X^h that satisfy the inclusion $X^h \subset C^1(\overline{\Omega})$, i.e., finding C^1 finite elements. As was discussed previously the Argyris finite element is an element of class C^1 and therefore will be the element of interest for the FE discretization of the SQGE.

4.3 LES Finite Element Formulation

In this section we will present the functional setting for the FE formulation of the the QGE (2.24) with LES applied to it. The FE formulation of the LES form of the QGE differs from the standard FE formulation of the QGE, because of the added closure model. Therefore, there should be an extra term corresponding to the closure model. This, I believe, will not change the functional space for the weak formulation and therefore will not change the functional space for the FE formulation. However, the error analysis that will be discussed in Section 5.3 will change due to the extra closure term.

4.4 Argyris Element

If we are to require conforming finite elements, Lagrange finite elements are not enough to guarantee continuity in the first derivative, and so to ensure continuity in the first derivative [29] the Argyris Element (depicted in Figure 4.1) will be required. The Argyris element is probably the best known of all C^1 finite elements [1, 14], but appear to be rarely implemented.

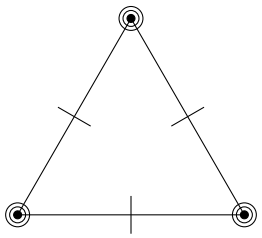

Figure 4.1: Argyris element with its 21 degrees of freedom.

The Argyris element does, in fact, ensure C^1 continuity [14, 40], but at a cost of twenty-one degrees of freedom. However, these twenty-one degrees of freedom give basis polynomials of degree five and therefore has a very high rate of convergence [14]. These degrees of freedom include the value at each vertex, the value of the first derivatives at each vertex, the value of the second derivatives at each vertex, the value of the mixed derivative at each vertex, and finally the value of the normal derivatives at each of the edge midpoints. Here in lies the main difficulty in implementing the Argyris triangle, the normal derivatives. Not only do we now have 21 degrees of freedom that we must worry about, but the added complexity of a transformation that maintains the direction of the normal derivatives is required. Since working on the reference element is the most common way of working with finite elements and normal derivatives are not respected by affine transformation a more complicated transformation will have to be employed. This is unlike a standard Lagrange element where only a simple Affine transformation is required. [14]

Dominguez *et al.* developed such a transformation. This transformation, which is a 21×21 matrix, C, allows for all calculations to be done on a reference element, vastly simplifying the calculations for the various matrices and load vector required for the QGE finite elements calculations and allowing for faster running code. Since, the tranformation of Dominguez is so new and is not the standard for implementation of the Argyris element his transformation will be discussed at length in Subsection 4.4.2 for completeness.

4.4.1 Basis Functions

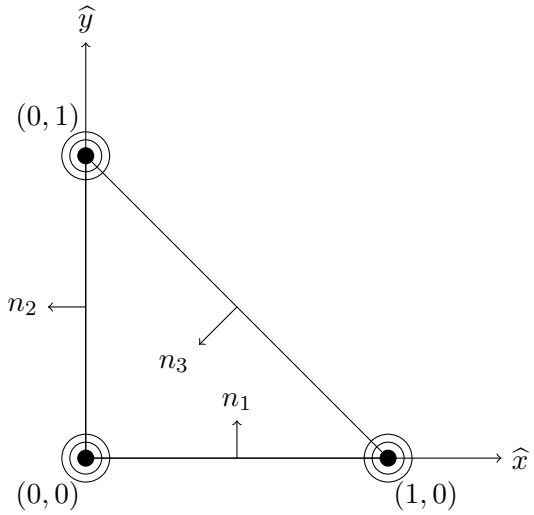

Figure 4.2: The reference triangle $\widehat{K}$ for Argyris

The Argyris triangle has 21 degrees of freedom and therefore has 21 basis functions per triangle. Additionally, the basis for Argyris in reference coordinates (depicted in Figure 4.2) belong to the space $\mathbb{P}_5$, which has the standard monomial basis

$$\left\{1, x, y, x^2, xy, y^2, x^3, x^2y, xy^2, y^3, x^4, x^3y, x^2y^2, xy^3, y^4, x^5, x^4y, x^3y^2, x^2y^3, xy^4, y^4\right\}$$

Thus, the i^{th} basis function for the Argyris triangle can be written as

$$\begin{aligned}\widehat{\varphi}_i(\widehat{x},\widehat{y}) = m_1^i + m_2^i\widehat{x} + m_3^i\widehat{x}^2 + m_4^i\widehat{x}^3 + m_5^i\widehat{x}^4 + m_6^i\widehat{x}^5 + m_7^i\widehat{y} + m_8^i\widehat{y}^2 + m_9^i\widehat{y}^3 \\ + m_{10}^i\widehat{y}^4 + m_{11}^i\widehat{y}^5 + m_{12}^i\widehat{x}\widehat{y} + m_{13}^i\widehat{x}\widehat{y}^2 + m_{14}^i\widehat{x}\widehat{y}^3 + m_{15}^i\widehat{x}\widehat{y}^4 + m_{16}^i\widehat{x}^2\widehat{y} \\ + m_{17}^i\widehat{x}^2\widehat{y}^2 + m_{18}^i\widehat{x}^2\widehat{y}^3 + m_{19}^i\widehat{x}^3\widehat{y} + m_{20}^i\widehat{x}^3\widehat{y}^2 + m_{21}^i\widehat{x}^4\widehat{y}\end{aligned} \tag{4.4}$$

Now, consider the reference triangle $\widehat{K}$ in Figure 4.2 with vertices numbered counter clockwise 1, 2, and 3, i.e. $(\widehat{x}_1,\widehat{y}_1) = (0,0)$, $(\widehat{x}_2,\widehat{y}_2) = (1,0)$, and $(\widehat{x}_3,\widehat{y}_3) = (0,1)$. Additionally, let the vector v_i represent the i^{th} edge with

$$v_1 = [\widehat{x}_2 - \widehat{x}_1, \widehat{y}_2 - \widehat{y}_1]^T, \quad v_2 = [\widehat{x}_3 - \widehat{x}_1, \widehat{y}_3 - \widehat{y}_1]^T \text{ and } v_3 = [\widehat{x}_3 - \widehat{x}_2, \widehat{y}_3 - \widehat{y}_2]^T.$$

Also, we will use the convention that the i^{th} normal vector is the rotation of the v_i counter-clockwise $90°$. Therefore, the i^{th} basis function can be found using the restriction in Table 4.4.1.

$i,j,k=1,2,3$	$i=4,5,6$ and $j,k=1,2,3$	$i=7,8,9$ and $j,k=1,2,3$
$\varphi_i(x_j,y_j)=\delta_{i,j}$ $\frac{\partial\varphi_i}{\partial x}(x_j,y_j)=0$ $\frac{\partial\varphi_i}{\partial y}(x_j,y_j)=0$ $\frac{\partial^2\varphi_i}{\partial x^2}(x_j,y_j)=0$ $\frac{\partial^2\varphi_i}{\partial x\partial y}(x_j,y_j)=0$ $\frac{\partial^2\varphi_i}{\partial y^2}(x_j,y_j)=0$ $\frac{\partial\varphi_i}{\partial n_k}=0$	$\varphi_i(x_j,y_j)=0$ $\frac{\partial\varphi_i}{\partial x}(x_j,y_j)=\delta_{i,j+3}$ $\frac{\partial\varphi_i}{\partial y}(x_j,y_j)=0$ $\frac{\partial^2\varphi_i}{\partial x^2}(x_j,y_j)=0$ $\frac{\partial^2\varphi_i}{\partial x\partial y}(x_j,y_j)=0$ $\frac{\partial^2\varphi_i}{\partial y^2}(x_j,y_j)=0$ $\frac{\partial\varphi_i}{\partial n_k}=0$	$\varphi_i(x_j,y_j)=0$ $\frac{\partial\varphi_i}{\partial x}(x_j,y_j)=0$ $\frac{\partial\varphi_i}{\partial y}(x_j,y_j)=\delta_{i,j+6}$ $\frac{\partial^2\varphi_i}{\partial x^2}(x_j,y_j)=0$ $\frac{\partial^2\varphi_i}{\partial x\partial y}(x_j,y_j)=0$ $\frac{\partial^2\varphi_i}{\partial y^2}(x_j,y_j)=0$ $\frac{\partial\varphi_i}{\partial n_k}=0$
$i=10,11,12$ and $j,k=1,2,3$	$i=13,14,15$ and $j,k=1,2,3$	$i=16,17,18$ and $j,k=1,2,3$
$\varphi_i(x_j,y_j)=0$ $\frac{\partial\varphi_i}{\partial x}(x_j,y_j)=0$ $\frac{\partial\varphi_i}{\partial y}(x_j,y_j)=0$ $\frac{\partial^2\varphi_i}{\partial x^2}(x_j,y_j)=\delta_{i,j+9}$ $\frac{\partial^2\varphi_i}{\partial x\partial y}(x_j,y_j)=0$ $\frac{\partial^2\varphi_i}{\partial y^2}(x_j,y_j)=0$ $\frac{\partial\varphi_i}{\partial n_k}=0$	$\varphi_i(x_j,y_j)=0$ $\frac{\partial\varphi_i}{\partial x}(x_j,y_j)=0$ $\frac{\partial\varphi_i}{\partial y}(x_j,y_j)=0$ $\frac{\partial^2\varphi_i}{\partial x^2}(x_j,y_j)=0$ $\frac{\partial^2\varphi_i}{\partial x\partial y}(x_j,y_j)=0$ $\frac{\partial^2\varphi_i}{\partial y^2}(x_j,y_j)=\delta_{i,j+12}$ $\frac{\partial\varphi_i}{\partial n_k}=0$	$\varphi_i(x_j,y_j)=0$ $\frac{\partial\varphi_i}{\partial x}(x_j,y_j)=0$ $\frac{\partial\varphi_i}{\partial y}(x_j,y_j)=0$ $\frac{\partial^2\varphi_i}{\partial x^2}(x_j,y_j)=0$ $\frac{\partial^2\varphi_i}{\partial x\partial y}(x_j,y_j)=\delta_{i,j+15}$ $\frac{\partial^2\varphi_i}{\partial y^2}(x_j,y_j)=0$ $\frac{\partial\varphi_i}{\partial n_k}=0$
	$i=19,20,21$ and $k=1,2,3$	
	$\varphi_i(x_j,y_j)=0$ $\frac{\partial\varphi_i}{\partial x}(x_j,y_j)=0$ $\frac{\partial\varphi_i}{\partial y}(x_j,y_j)=0$ $\frac{\partial^2\varphi_i}{\partial x^2}(x_j,y_j)=0$ $\frac{\partial^2\varphi_i}{\partial x\partial y}(x_j,y_j)=0$ $\frac{\partial^2\varphi_i}{\partial y^2}(x_j,y_j)=0$ $\frac{\partial\varphi_i}{\partial n_k}=\delta_{i,k-18}$	

Table 4.1: Constraints for Argyris triangle

Now, let z be the vector containing the monomial basis for $\mathbb{P}_5$, i.e.

$$z=\left[1,\widehat{x},\widehat{y},\widehat{x}^2,\widehat{x}\widehat{y},\widehat{y}^2,\widehat{x}^3,\widehat{x}^2\widehat{y},\widehat{x}\widehat{y}^2,\widehat{y}^3,\widehat{x}^4,\widehat{x}^3\widehat{y},\widehat{x}^2\widehat{y}^2,\widehat{x}\widehat{y}^3,\widehat{y}^4,\widehat{x}^5,\widehat{x}^4\widehat{y},\widehat{x}^3\widehat{y}^2,\widehat{x}^2\widehat{y}^3,\widehat{x}\widehat{y}^4,\widehat{y}^4\right]^T$$

Then the i^{th} Argyris basis function on $\widehat{K}$ is given by

$$\widehat{\varphi}_i=M_iz,$$

where M_i is the i^{th} row of the matrix M. Therefore, the evaluation of $\widehat{\varphi}_i(\widehat{x},\widehat{y})$ comes down to the matrix-vector multiplication

$$\widehat{\varphi}_i(\widehat{x},\widehat{y}) = M_i z(\widehat{x},\widehat{y}).$$

To determine the matrix M we must solve the linear system

$$ZM^T = I_{21}$$

that result from the constraints in Table 4.4.1. Here

$$\begin{aligned} Z = [&z(0,0), z(0,1), z(1,0), z_{\widehat{x}}(0,0), z_{\widehat{y}}(0,0), z_{\widehat{x}}(1,0), z_{\widehat{y}}(1,0), z_{\widehat{x}}(0,1), z_{\widehat{y}}(0,1),\\ &z_{\widehat{x}\widehat{x}}(0,0), z_{\widehat{x}\widehat{y}}(0,0), z_{\widehat{y}\widehat{y}}(0,0), z_{\widehat{x}\widehat{x}}(1,0), z_{\widehat{x}\widehat{y}}(1,0), z_{\widehat{y}\widehat{y}}(1,0),\\ &z_{\widehat{x}\widehat{x}}(0,1), z_{\widehat{x}\widehat{y}}(0,1), z_{\widehat{y}\widehat{y}}(0,1), z_{\widehat{y}}(1/2,0), -z_{\widehat{x}}(0,1/2),\\ &-\frac{1}{\sqrt{2}}(z_{\widehat{x}}(1/2,1/2) + z_{\widehat{y}}(1/2,1/2))]^T \end{aligned}$$

I_{21} is a 21×21 identity matrix and M is the matrix containing the coefficients for all 21 basis functions. Therefore solving this system will result in a matrix, M, that contains the coefficients for the Argyris basis functions for the reference triangle as in (4.4). Thus, the matrix M is

$$\begin{bmatrix}
1 & 0 & 0 & 0 & 0 & 0 & -10 & 0 & 0 & -10 & 15 & 0 & -30 & 0 & 15 & -6 & 0 & 30 & 30 & 0 & -6 \\
0 & 0 & 0 & 0 & 0 & 0 & 10 & 0 & 0 & 0 & -15 & 0 & 15 & 0 & 0 & 6 & 0 & -15 & -15 & 0 & 0 \\
0 & 0 & 0 & 0 & 0 & 0 & 0 & 0 & 0 & 10 & 0 & 0 & 15 & 0 & -15 & 0 & 0 & -15 & -15 & 0 & 6 \\
0 & 1 & 0 & 0 & 0 & 0 & -6 & 0 & -11 & 0 & 8 & 0 & 10 & 18 & 0 & -3 & 0 & 1 & -10 & -8 & 0 \\
0 & 0 & 1 & 0 & 0 & 0 & 0 & -11 & 0 & -6 & 0 & 18 & 10 & 0 & 8 & 0 & -8 & -10 & 1 & 0 & -3 \\
0 & 0 & 0 & 0 & 0 & 0 & -4 & 0 & 0 & 0 & 7 & 0 & $-\frac{7}{2}$ & 0 & 0 & -3 & 0 & $\frac{7}{2}$ & $\frac{7}{2}$ & 0 & 0 \\
0 & 0 & 0 & 0 & 0 & 0 & 0 & -5 & 0 & 0 & 0 & 14 & $\frac{37}{2}$ & 0 & 0 & 0 & -8 & $-\frac{37}{2}$ & $-\frac{27}{2}$ & 0 & 0 \\
0 & 0 & 0 & 0 & 0 & 0 & 0 & 0 & -5 & 0 & 0 & 0 & $\frac{37}{2}$ & 14 & 0 & 0 & 0 & $-\frac{27}{2}$ & $-\frac{37}{2}$ & -8 & 0 \\
0 & 0 & 0 & 0 & 0 & 0 & 0 & 0 & 0 & -4 & 0 & 0 & $-\frac{7}{2}$ & 0 & 7 & 0 & 0 & $\frac{7}{2}$ & $\frac{7}{2}$ & 0 & -3 \\
0 & 0 & 0 & $\frac{1}{2}$ & 0 & 0 & $-\frac{3}{2}$ & 0 & 0 & 0 & $\frac{3}{2}$ & 0 & $-\frac{3}{2}$ & 0 & 0 & $-\frac{1}{2}$ & 0 & $\frac{3}{2}$ & 1 & 0 & 0 \\
0 & 0 & 0 & 0 & 1 & 0 & 0 & -4 & -4 & 0 & 0 & 5 & 10 & 5 & 0 & 0 & -2 & -6 & -6 & -2 & 0 \\
0 & 0 & 0 & 0 & 0 & $\frac{1}{2}$ & 0 & 0 & 0 & $-\frac{3}{2}$ & 0 & 0 & $-\frac{3}{2}$ & 0 & $\frac{3}{2}$ & 0 & 0 & 1 & $\frac{3}{2}$ & 0 & $-\frac{1}{2}$ \\
0 & 0 & 0 & 0 & 0 & 0 & $\frac{1}{2}$ & 0 & 0 & 0 & -1 & 0 & $\frac{1}{4}$ & 0 & 0 & $\frac{1}{2}$ & 0 & $-\frac{1}{4}$ & $-\frac{1}{4}$ & 0 & 0 \\
0 & 0 & 0 & 0 & 0 & 0 & 0 & 1 & 0 & 0 & 0 & -3 & $-\frac{7}{2}$ & 0 & 0 & 0 & 2 & $\frac{7}{2}$ & $\frac{5}{2}$ & 0 & 0 \\
0 & 0 & 0 & 0 & 0 & 0 & 0 & 0 & 0 & 0 & 0 & 0 & $\frac{5}{4}$ & 0 & 0 & 0 & 0 & $-\frac{3}{4}$ & $-\frac{5}{4}$ & 0 & 0 \\
0 & 0 & 0 & 0 & 0 & 0 & 0 & 0 & 0 & 0 & 0 & 0 & $\frac{5}{4}$ & 0 & 0 & 0 & 0 & $-\frac{5}{4}$ & $-\frac{3}{4}$ & 0 & 0 \\
0 & 0 & 0 & 0 & 0 & 0 & 0 & 0 & 1 & 0 & 0 & 0 & $-\frac{7}{2}$ & -3 & 0 & 0 & 0 & $\frac{5}{2}$ & $\frac{7}{2}$ & 2 & 0 \\
0 & 0 & 0 & 0 & 0 & 0 & 0 & 0 & 0 & $\frac{1}{2}$ & 0 & 0 & $\frac{1}{4}$ & 0 & -1 & 0 & 0 & $-\frac{1}{4}$ & $-\frac{1}{4}$ & 0 & $\frac{1}{2}$ \\
0 & 0 & 0 & 0 & 0 & 0 & 0 & 16 & 0 & 0 & 0 & -32 & -32 & 0 & 0 & 0 & 16 & 32 & 16 & 0 & 0 \\
0 & 0 & 0 & 0 & 0 & 0 & 0 & 0 & -16 & 0 & 0 & 0 & 32 & 32 & 0 & 0 & 0 & -16 & -32 & -16 & 0 \\
0 & 0 & 0 & 0 & 0 & 0 & 0 & 0 & 0 & 0 & 0 & 0 & $8\sqrt{2}$ & 0 & 0 & 0 & 0 & $-8\sqrt{2}$ & $-8\sqrt{2}$ & 0 & 0
\end{bmatrix}$$

Table 4.2: Coefficients for the Argyris Basis Matrix, M

Therefore, the Argyris basis functions are

$$
\begin{aligned}
\widehat{\varphi}_1(\widehat{x},\widehat{y}) &= 1 - 10\widehat{x}^3 - 10\widehat{y}^3 + 15\widehat{x}^4 - 30\widehat{x}^2\widehat{y}^2 + 15\widehat{y}^4 - 6\widehat{x}^5 + 30\widehat{x}^3\widehat{y}^2 + 30\widehat{x}^2\widehat{y}^3 - 6\widehat{y}^5\\
\widehat{\varphi}_2(\widehat{x},\widehat{y}) &= 10\widehat{x}^3 - 15\widehat{x}^4 + 15\widehat{x}^2\widehat{y}^2 + 6\widehat{x}^5 - 15\widehat{x}^3\widehat{y}^2 - 15\widehat{x}^2\widehat{y}^3\\
\widehat{\varphi}_3(\widehat{x},\widehat{y}) &= 10\widehat{y}^3 + 15\widehat{x}^2\widehat{y}^2 - 15\widehat{y}^4 - 15\widehat{x}^3\widehat{y}^2 - 15\widehat{x}^2\widehat{y}^3 + 6\widehat{y}^2\\
\widehat{\varphi}_4(\widehat{x},\widehat{y}) &= \widehat{x} - 6\widehat{x}^3 - 11\widehat{x}\widehat{y}^2 + 8\widehat{x}^4 + 10\widehat{x}^2\widehat{y}^2 + 18\widehat{x}\widehat{y}^3 - 3\widehat{x}^5 + \widehat{x}^3\widehat{y}^2 - 10\widehat{x}^2\widehat{y}^3 - 8\widehat{x}\widehat{y}^4\\
\widehat{\varphi}_5(\widehat{x},\widehat{y}) &= \widehat{y} - 11\widehat{x}^2\widehat{y} - 6\widehat{y}^3 + 18\widehat{x}^3\widehat{y} + 10\widehat{x}^2\widehat{y}^2 + 8\widehat{y}^4 - 8\widehat{x}^4\widehat{y} - 10\widehat{x}^3\widehat{y}^2 + \widehat{x}^2\widehat{y}^3 - 3\widehat{y}^5\\
\widehat{\varphi}_6(\widehat{x},\widehat{y}) &= -4\widehat{x}^3 + 7\widehat{x}^4 - \frac{7}{2}\widehat{x}^2\widehat{y}^2 - 3\widehat{x}^5 + \frac{7}{2}\widehat{x}^3\widehat{y}^2 + \frac{7}{2}\widehat{x}^2\widehat{y}^3\\
\widehat{\varphi}_7(\widehat{x},\widehat{y}) &= -5\widehat{x}^2\widehat{y} + 14\widehat{x}^3\widehat{y} + \frac{37}{2}\widehat{x}^2\widehat{y}^2 - 8\widehat{x}^4\widehat{y} - \frac{37}{2}\widehat{x}^3\widehat{y}^2 - \frac{27}{2}\widehat{x}^2\widehat{y}^3\\
\widehat{\varphi}_8(\widehat{x},\widehat{y}) &= -5\widehat{x}\widehat{y}^2 + \frac{37}{2}\widehat{x}^2\widehat{y}^2 + 14\widehat{x}\widehat{y}^3 - \frac{27}{2}\widehat{x}^3\widehat{y}^2 - \frac{37}{2}\widehat{x}^3\widehat{y}^2 - 8\widehat{x}\widehat{y}^4\\
\widehat{\varphi}_9(\widehat{x},\widehat{y}) &= -4\widehat{y}^3 - \frac{7}{2}\widehat{x}^3 + 7\widehat{y}^4 + \frac{7}{2}\widehat{x}^3\widehat{y}^2 + \frac{7}{2}\widehat{x}^2\widehat{y}^3 - 3\widehat{y}^5\\
\widehat{\varphi}_{10}(\widehat{x},\widehat{y}) &= \frac{1}{2}\widehat{x}^2 - \frac{3}{2}\widehat{x}^3 + \frac{3}{2}\widehat{x}^4 - \frac{3}{2}\widehat{x}^2\widehat{y}^2 - \frac{1}{2}\widehat{x}^5 + \frac{3}{2}\widehat{x}^3\widehat{y}^2 + \widehat{x}^2\widehat{y}^3\\
\widehat{\varphi}_{11}(\widehat{x},\widehat{y}) &= \widehat{x}\widehat{y} - 4\widehat{x}^2\widehat{y} - 4\widehat{x}\widehat{y}^2 + 5\widehat{x}^3\widehat{y} + 10\widehat{x}^2\widehat{y}^2 + 5\widehat{x}\widehat{y}^3 - 2\widehat{x}^4\widehat{y} - 6\widehat{x}^3\widehat{y}^2 - 6\widehat{x}^2\widehat{y}^3 - 2\widehat{x}\widehat{y}^4\\
\widehat{\varphi}_{12}(\widehat{x},\widehat{y}) &= \frac{1}{2}\widehat{y}^2 - \frac{3}{2}\widehat{y}^3 - \frac{3}{2}\widehat{x}^2\widehat{y}^2 + \frac{3}{2}\widehat{y}^4 + \widehat{x}^3\widehat{y}^2 + \frac{3}{2}\widehat{x}^2\widehat{y}^3 - \frac{1}{2}\widehat{y}^5\\
\widehat{\varphi}_{13}(\widehat{x},\widehat{y}) &= \frac{1}{2}\widehat{x}^3 - \widehat{x}^4 + \frac{1}{4}\widehat{x}^2\widehat{y}^2 + \frac{1}{2}\widehat{x}^5 - \frac{1}{4}\widehat{x}^3\widehat{y}^2 - \frac{1}{4}\widehat{x}^2\widehat{y}^3\\
\widehat{\varphi}_{14}(\widehat{x},\widehat{y}) &= \widehat{x}^2\widehat{y} - 3\widehat{x}^3\widehat{y} - \frac{7}{2}\widehat{x}^2\widehat{y}^2 + 2\widehat{x}^4\widehat{y} + \frac{7}{2}\widehat{x}^3\widehat{y}^2 + \frac{5}{2}\widehat{x}^2\widehat{y}^3\\
\widehat{\varphi}_{15}(\widehat{x},\widehat{y}) &= \frac{5}{4}\widehat{x}^2\widehat{y}^2 - \frac{3}{4}\widehat{x}^3\widehat{y}^2 - \frac{5}{4}\widehat{x}^2\widehat{y}^3\\
\widehat{\varphi}_{16}(\widehat{x},\widehat{y}) &= \frac{5}{4}\widehat{x}^2\widehat{y}^2 - \frac{5}{4}\widehat{x}^3\widehat{y}^2 - \frac{3}{4}\widehat{x}^2\widehat{y}^3\\
\widehat{\varphi}_{17}(\widehat{x},\widehat{y}) &= \widehat{x}\widehat{y}^2 - \frac{7}{2}\widehat{x}^2\widehat{y}^2 - 3\widehat{x}\widehat{y}^3 + \frac{5}{2}\widehat{x}^3\widehat{y}^2 + \frac{7}{2}\widehat{x}^2\widehat{y}^3 + 2\widehat{x}\widehat{y}^4\\
\widehat{\varphi}_{18}(\widehat{x},\widehat{y}) &= \frac{1}{2}\widehat{y}^3 + \frac{1}{4}\widehat{x}^2\widehat{y}^2 - \widehat{y}^4 - \frac{1}{4}\widehat{x}^3\widehat{y}^2 - \frac{1}{4}\widehat{x}^2\widehat{y}^3 + \frac{1}{2}\widehat{y}^5\\
\widehat{\varphi}_{19}(\widehat{x},\widehat{y}) &= 16\widehat{x}^2\widehat{y} - 32\widehat{x}^3\widehat{y} - 32\widehat{x}^2\widehat{y}^2 + 16\widehat{x}^4\widehat{y} + 32\widehat{x}^3\widehat{y}^2 + 16\widehat{x}^2\widehat{y}^3\\
\widehat{\varphi}_{20}(\widehat{x},\widehat{y}) &= -16\widehat{x}\widehat{y}^2 + 32\widehat{x}^2\widehat{y}^2 + 32\widehat{x}\widehat{y}^3 - 16\widehat{x}^3\widehat{y}^2 - 32\widehat{x}^2\widehat{y}^3 - 16\widehat{x}\widehat{y}^4\\
\widehat{\varphi}_{21}(\widehat{x},\widehat{y}) &= \sqrt{2}\left(8\widehat{x}^2\widehat{y}^2 - 8\widehat{x}^3\widehat{y}^2 - 8\widehat{x}^2\widehat{y}^3\right)
\end{aligned}
\tag{4.5}
$$

4.4.2 Transformation

Now that we have the Argyris basis functions on the reference triangle we need to relate those to the Argyris basis functions on a general triangle. So let's first consider the affine transformation from $\widehat{K}$ to K, i.e. $F : \widehat{K} \to K$ such that

$$
F(\widehat{\mathbf{x}}) = B\widehat{\mathbf{x}} + \mathbf{b} := \begin{bmatrix} x_2 - x_1 & x_3 - x_1 \\ y_2 - y_1 & y_3 - y_1 \end{bmatrix} \begin{bmatrix} \widehat{x} \\ \widehat{y} \end{bmatrix} + \begin{bmatrix} x_1 \\ y_1 \end{bmatrix}. \tag{4.6}
$$

Also number the vectors representing the edge of the triangle as

$$
\mathbf{v}_1 = \mathbf{x}_2 - \mathbf{x}_1 \quad \mathbf{v}_2 = \mathbf{x}_3 - \mathbf{x}_1 \quad \mathbf{v}_3 = \mathbf{x}_3 - \mathbf{x}_2
$$

Let $\mathbf{n}_i$ be the unit normal vector corresponding to the i^{th} side obtained by rotating the vector $\mathbf{v}_i$ by $\pi/2$ in the positive direction. Additionally, let $\mathbf{m}_i$ be the midpoint to the i^{th} side. Now consider the linear functionals

corresponding to the vertices of the triangle K numbered as

$$\begin{aligned}
&\mathcal{L}_i(\varphi) := \varphi(\mathbf{x}_i),\\
&\mathcal{L}_i^\circ(\varphi) := \partial_\circ\varphi(\mathbf{x}_i) \quad \circ \in \{x, y\},\\
&\mathcal{L}_i^\circ(\varphi) := \partial_\circ\varphi(\mathbf{x}_i) \quad \circ \in \{xx, xy, yy\}
\end{aligned}$$

for $i \in \{1, 2, 3\}$. For the functionals corresponding to the sides

$$\mathcal{L}_i^n(\varphi) := \nabla_{\mathbf{x}}\phi(\mathbf{m}_i) \cdot \mathbf{n}_i \quad i \in \{1, 2, 3\}.$$

Now let's renumber the linear functionals as $\mathcal{L}_j$ for $j \in \{1, \ldots, 21\}$ as they are listed below

$$\begin{aligned}
&\mathcal{L}_1, \mathcal{L}_2, \mathcal{L}_3,\\
&\mathcal{L}_1^x, \mathcal{L}_1^y, \mathcal{L}_2^x, \mathcal{L}_2^y, \mathcal{L}_3^x, \mathcal{L}_3^y,\\
&\mathcal{L}_1^{xx}, \mathcal{L}_1^{xy}, \mathcal{L}_1^{yy}, \mathcal{L}_2^{xx}, \mathcal{L}_2^{xy}, \mathcal{L}_2^{yy}, \mathcal{L}_3^{xx}, \mathcal{L}_3^{xy}, \mathcal{L}_3^{yy},\\
&\mathcal{L}_1^n, \mathcal{L}_2^n, \mathcal{L}_3^n,
\end{aligned}$$

and the linear functionals $\widehat{\mathcal{L}}_i$ and $\widehat{\mathcal{L}_i^n}$ are the corresponding functionals on the reference triangle $\widehat{K}$. The basis functions of the Argyris triangle are fifth degree polynomials in $\mathbb{P}_5(K)$ that satisfy

$$\mathcal{L}_i(\varphi_j) = \delta_{ij} \quad i, j \in \{1, \ldots, 21\}$$

and similarly on the reference triangle

$$\widehat{\mathcal{L}}_i(\widehat{\varphi}_j) = \delta_{ij} \quad i, j \in \{1, \ldots, 21\}.$$

Now define a new set of functionals such that

$$\widetilde{\mathcal{L}}_i(\varphi) := \widehat{\mathcal{L}}_i(\varphi \circ F). \tag{4.7}$$

Since $\{\widetilde{\mathcal{L}}_i\}$ and $\{\widehat{\mathcal{L}}_i\}$ are both basis for the dual space of $\mathbb{P}_5(K)$ there is a nonsingular matrix C such that

$$\widetilde{\mathcal{L}}_i = \sum_{j=1}^{21} c_{ij}\mathcal{L}_j \quad i \in \{1, \ldots, 21\}. \tag{4.8}$$

and therefore it follows

$$\varphi_i \circ F = \sum_{j=1}^{21} c_{ij}\widehat{\varphi}_j \quad i \in \{1, \ldots, 21\}. \tag{4.9}$$

[14] Now, we must determine a simple expression for this C.

Let's introduce a new set of linear functionals

$$\mathcal{L}_i^* \quad i \in \{1, \ldots, 24\}$$

in the following way; first we let $\mathcal{L}_i^* := \mathcal{L}_i$ $i = \{1, \ldots, 18\}$ and then introduce the new functionals

$$\mathcal{L}_i^\circ \quad \circ \in \{\perp, ||\} \quad i \in \{1, 2, 3\}$$

by the following relationship

$$\mathcal{L}_i^\perp(\varphi) := \nabla_{\mathbf{x}}\varphi(\mathbf{m}_i) \cdot R\mathbf{v}_i, \quad \mathcal{L}_i^{||}(\varphi) := \nabla_{\mathbf{x}}\varphi(\mathbf{m}_i) \cdot \mathbf{v}_i$$

where

$$R = \begin{bmatrix} 0 & -1 \\ 1 & 0 \end{bmatrix}$$

is the matrix that rotates a vector $\pi/2$ counter-clockwise. Now order the linear functionals as $\mathcal{L}_1^{\perp}, \mathcal{L}_2^{\perp}, \mathcal{L}_3^{\perp}, \mathcal{L}_1^{||}, \mathcal{L}_2^{||}, \mathcal{L}_3^{||}$. Therefore, we have the relationship

$$\widetilde{\mathcal{L}}_i = \sum_{j=1}^{24} d_{ij}\mathcal{L}_j^*, \quad i \in \{1, \ldots, 21\}. \tag{4.10}$$

Now from (4.6) we see that

$$\begin{aligned} \frac{\partial x}{\partial \widehat{x}} &= B_{11} & \frac{\partial x}{\partial \widehat{y}} &= B_{12} \\ \frac{\partial y}{\partial \widehat{x}} &= B_{21} & \frac{\partial y}{\partial \widehat{y}} &= B_{22} \end{aligned}$$

With this we can determine the relationship between the gradient of $\widehat{\varphi}$ on the triangle $\widehat{K}$ to the gradient of φ on the triangle K

$$\begin{aligned} \nabla_{\widehat{\mathbf{x}}} (\varphi \circ F) &= \begin{bmatrix} \dfrac{\partial \varphi \circ F}{\partial \widehat{x}} \\ \dfrac{\partial \varphi \circ F}{\partial \widehat{y}} \end{bmatrix} \\ &= \begin{bmatrix} \dfrac{\partial \varphi \circ F}{\partial x} \cdot \dfrac{\partial x}{\partial \widehat{x}} + \dfrac{\partial \varphi \circ F}{\partial y} \cdot \dfrac{\partial y}{\partial \widehat{x}} \\ \dfrac{\partial \varphi \circ F}{\partial x} \cdot \dfrac{\partial x}{\partial \widehat{y}} + \dfrac{\partial \varphi \circ F}{\partial y} \cdot \dfrac{\partial y}{\partial \widehat{y}} \end{bmatrix} \\ &= \begin{bmatrix} \dfrac{\partial x}{\partial \widehat{x}} & \dfrac{\partial y}{\partial \widehat{x}} \\ \dfrac{\partial x}{\partial \widehat{y}} & \dfrac{\partial y}{\partial \widehat{y}} \end{bmatrix} \cdot \begin{bmatrix} \dfrac{\partial \varphi \circ F}{\partial x} \\ \dfrac{\partial \varphi \circ F}{\partial y} \end{bmatrix} \end{aligned}$$

and so

$$\nabla_{\widehat{\mathbf{x}}} (\varphi \circ F) = B^T \nabla_{\mathbf{x}} \varphi \circ F \tag{4.11}$$

If we defined the Hessian as $H_x(\varphi) = [\varphi_{xx}, \varphi_{xy}, \varphi_{yy}]^T$ then using (4.6) we can determine the relationship

between the hessian of $\widehat{\varphi}$ on the triangle $\widehat{K}$ to the hessian of φ on the triangle K

$$\begin{aligned}
H_{\widehat{\mathbf{x}}}(\varphi \circ F) &= \begin{bmatrix} \dfrac{\partial^2 \varphi \circ F}{\partial \widehat{x}^2} \\ \dfrac{\partial^2 \varphi \circ F}{\partial \widehat{x} \partial \widehat{y}} \\ \dfrac{\partial^2 \varphi \circ F}{\partial \widehat{y}^2} \end{bmatrix} \\
&= \begin{bmatrix} \dfrac{\partial}{\partial \widehat{x}} \left(\dfrac{\partial \varphi \circ F}{\partial x} \cdot \dfrac{\partial x}{\partial \widehat{x}} + \dfrac{\partial \varphi \circ F}{\partial y} \cdot \dfrac{\partial y}{\partial \widehat{x}} \right) \\ \dfrac{\partial}{\partial \widehat{y}} \left(\dfrac{\partial \varphi \circ F}{\partial x} \cdot \dfrac{\partial x}{\partial \widehat{x}} + \dfrac{\partial \varphi \circ F}{\partial y} \cdot \dfrac{\partial y}{\partial \widehat{x}} \right) \\ \dfrac{\partial}{\partial \widehat{y}} \left(\dfrac{\partial \varphi \circ F}{\partial x} \cdot \dfrac{\partial x}{\partial \widehat{y}} + \dfrac{\partial \varphi \circ F}{\partial y} \cdot \dfrac{\partial y}{\partial \widehat{y}} \right) \end{bmatrix} \\
&= \begin{bmatrix} \dfrac{\partial^2 \varphi \circ F}{\partial x^2} \cdot \left(\dfrac{\partial x}{\partial \widehat{x}} \right)^2 + 2 \dfrac{\partial^2 \varphi \circ F}{\partial x \partial y} \cdot \dfrac{\partial x}{\partial \widehat{x}} \cdot \dfrac{\partial y}{\partial \widehat{x}} + \dfrac{\partial \varphi \circ F}{\partial y^2} \cdot \left(\dfrac{\partial y}{\partial \widehat{x}} \right)^2 \\ \dfrac{\partial^2 \varphi \circ F}{\partial x^2} \cdot \dfrac{\partial x}{\partial \widehat{x}} \cdot \dfrac{\partial x}{\partial \widehat{y}} + \left(\dfrac{\partial x}{\partial \widehat{x}} \cdot \dfrac{\partial y}{\partial \widehat{y}} + \dfrac{\partial x}{\partial \widehat{y}} \cdot \dfrac{\partial y}{\partial \widehat{x}} \right) \dfrac{\partial^2 \varphi \circ F}{\partial x \partial y} + \dfrac{\partial \varphi \circ F}{\partial y^2} \cdot \dfrac{\partial y}{\partial \widehat{x}} \cdot \dfrac{\partial y}{\partial \widehat{y}} \\ \dfrac{\partial^2 \varphi \circ F}{\partial x^2} \cdot \left(\dfrac{\partial x}{\partial \widehat{y}} \right)^2 + 2 \dfrac{\partial^2 \varphi \circ F}{\partial x \partial \widehat{y}} \cdot \dfrac{\partial x}{\partial \widehat{y}} \cdot \dfrac{\partial y}{\partial \widehat{y}} + \dfrac{\partial \varphi \circ F}{\partial y^2} \cdot \left(\dfrac{\partial y}{\partial \widehat{y}} \right)^2 \end{bmatrix}
\end{aligned}$$

$$= \begin{bmatrix} \left(\dfrac{\partial x}{\partial \widehat{x}} \right)^2 & 2 \dfrac{\partial x}{\partial \widehat{x}} \cdot \dfrac{\partial y}{\partial \widehat{x}} & \left(\dfrac{\partial y}{\partial \widehat{x}} \right)^2 \\ \dfrac{\partial x}{\partial \widehat{x}} \cdot \dfrac{\partial x}{\partial \widehat{y}} & \left(\dfrac{\partial x}{\partial \widehat{x}} \cdot \dfrac{\partial y}{\partial \widehat{y}} + \dfrac{\partial x}{\partial \widehat{y}} \cdot \dfrac{\partial y}{\partial \widehat{x}} \right) & \dfrac{\partial y}{\partial \widehat{x}} \cdot \dfrac{\partial y}{\partial \widehat{y}} \\ \left(\dfrac{\partial x}{\partial \widehat{y}} \right)^2 & 2 \dfrac{\partial x}{\partial \widehat{y}} \cdot \dfrac{\partial y}{\partial \widehat{y}} & \left(\dfrac{\partial y}{\partial \widehat{y}} \right)^2 \end{bmatrix} \cdot \begin{bmatrix} \dfrac{\partial^2 \varphi \circ F}{\partial x^2} \\ \dfrac{\partial^2 \varphi \circ F}{\partial x \partial y} \\ \dfrac{\partial^2 \varphi \circ F}{\partial y^2} \end{bmatrix}$$

and so

$$H_{\widehat{\mathbf{x}}}(\varphi \circ F) = \Theta H_{\mathbf{x}}(\varphi) \circ F \tag{4.12}$$

where

$$\Theta = \begin{bmatrix} B_{11}^2 & 2B_{11}B_{21} & B_{21}^2 \\ B_{12}B_{11} & B_{12}B_{21} + B_{11}B_{22} & B_{21}B_{22} \\ B_{12}^2 & 2B_{22}B_{12} & B_{22}^2 \end{bmatrix}.$$

Therefore we see that

$$\widetilde{\mathcal{L}}_i = \mathcal{L}_i, \quad \begin{bmatrix} \widetilde{\mathcal{L}}_i^x \\ \widetilde{\mathcal{L}}_i^y \end{bmatrix} = B^T \begin{bmatrix} \mathcal{L}_i^x \\ \mathcal{L}_i^y \end{bmatrix}, \quad \begin{bmatrix} \widetilde{\mathcal{L}}_i^{xx} \\ \widetilde{\mathcal{L}}_i^{xy} \\ \widetilde{\mathcal{L}}_i^{yy} \end{bmatrix} = \Theta \begin{bmatrix} \mathcal{L}_i^{xx} \\ \mathcal{L}_i^{xy} \\ \mathcal{L}_i^{yy} \end{bmatrix}$$

Additionally, notice $\mathbf{v}_i = B\widehat{\mathbf{v}}_i$ for $i = \{1, 2, 3\}$ where $\widehat{\mathbf{v}}_i$ are defined on the reference triangle $\widehat{K}$. It should also be noted that

$$\begin{bmatrix} \mathcal{L}_i^{\perp} \\ \mathcal{L}_i^{||} \end{bmatrix} = \begin{bmatrix} -v_i^y & v_i^x \\ v_i^x & v_i^y \end{bmatrix} \begin{bmatrix} \mathcal{L}_i^x \\ \mathcal{L}_i^y \end{bmatrix}$$

and therefore

$$\begin{bmatrix} \mathcal{L}_i^x \\ \mathcal{L}_i^y \end{bmatrix} = \frac{1}{|v_i|^2} \begin{bmatrix} -v_i^y & v_i^x \\ v_i^x & v_i^y \end{bmatrix} \begin{bmatrix} \mathcal{L}_i^{\perp} \\ \mathcal{L}_i^{||} \end{bmatrix}.$$

Then

$$\begin{aligned}\widetilde{\mathcal{L}}_i^n(\varphi) &= \widehat{\mathcal{L}}_i^n(\varphi \circ F) \\ &= \frac{1}{|\widehat{\mathbf{v}}_i|} R\widehat{\mathbf{v}}_i \cdot \nabla_{\widehat{\mathbf{x}}}(\varphi \circ F)(\widehat{\mathbf{m}}_i) \\ &= \frac{1}{|\widehat{\mathbf{v}}_i|} R\widehat{\mathbf{v}}_i \cdot B^T \nabla_{\mathbf{x}} \varphi(\mathbf{m}_i) \\ &= \frac{1}{|\widehat{\mathbf{v}}_i|} R\widehat{\mathbf{v}}_i \cdot \ell_i^{-2} B^T \begin{bmatrix} -v_i^y & v_i^x \\ v_i^x & v_i^y \end{bmatrix} \begin{bmatrix} \mathcal{L}_i^{\perp} \\ \mathcal{L}_i^{||} \end{bmatrix}\end{aligned}$$

where ℓ_i is the length of the i^{th} side. This can be written in the form

$$\widetilde{\mathcal{L}}_i^n = f_i \mathcal{L}_i^{\perp} + g_i \mathcal{L}_i^{||},$$

where

$$f_i = \frac{1}{\ell_i^2 |\widehat{\mathbf{v}}_i|} R\widehat{\mathbf{v}}_i \cdot B^T R\mathbf{v}_i \quad g_i = \frac{1}{\ell_i^2 |\widehat{\mathbf{v}}_i|} R\widehat{\mathbf{v}}_i \cdot B^T \mathbf{v}_i.$$

Therefore, we can construct a 21×24 the matrix D in block diagonal form in the following way

$$D = \text{diag}[I_3, B^T, B^T, B^T, \Theta, \Theta, \Theta, Q]$$

where

$$Q = \left[\begin{array}{ccc|ccc} f_1 & & & g_1 & & \\ & f_2 & & & g_2 & \\ & & f_3 & & & g_3 \end{array}\right]$$

It also holds that

$$\mathcal{L}_i^* = \sum_{j=1}^{21} e_{ij} \mathcal{L}_j \quad i \in \{1, \ldots, 24\}. \tag{4.13}$$

It should be clear that $\mathcal{L}_i^* = \mathcal{L}_i$ for $i = 1, \ldots, 18$ and since $\ell_i \mathbf{n}_i = R\mathbf{v}_i$ we see that $\mathcal{L}_i^{\perp} = \ell_i \mathcal{L}_i^n$. Now let ϕ be an arbitrary polynomial in $\mathbb{P}_5(K)$ and define

$$\psi(t) := \varphi(t\mathbf{x}_\beta + (1-t)\mathbf{x}_\alpha) \in \mathbb{P}_5(t) \; \alpha < \beta$$

then

$$\psi'(1/2) = \frac{15}{8}(\psi(1) - \psi(0)) - \frac{7}{16}(\psi'(1) + \psi'(0)) + \frac{1}{32}(\psi''(1) - \psi''(0)) \tag{4.14}$$

Taking γ to be the index corresponding to $\mathbf{v}_\gamma = \mathbf{x}_\beta - \mathbf{x}_\alpha$ and since

$$\begin{aligned}\psi'(1/2) &= \mathcal{L}_\gamma(\varphi) \\ \psi(0) &= \mathcal{L}_\alpha(\varphi) \\ \psi(1) &= \mathcal{L}_\beta(\varphi) \\ \psi'(0) &= v_\gamma^x \mathcal{L}_\alpha^x(\varphi) + v_\gamma^y \mathcal{L}_\alpha^y(\varphi) \\ \psi'(1) &= v_\gamma^x \mathcal{L}_\beta^x(\varphi) + v_\gamma^y \mathcal{L}_\beta^y(\varphi) \\ \psi''(0) &= (v_\gamma^x)^2 \mathcal{L}_\alpha^{xx}(\varphi) + 2v_\gamma^x v_\gamma^y \mathcal{L}_\alpha^{xy}(\varphi) + (v_\gamma^y)^2 \mathcal{L}_\alpha^{yy}(\varphi) \\ \psi''(1) &= (v_\gamma^x)^2 \mathcal{L}_\beta^{xx}(\varphi) + 2v_\gamma^x v_\gamma^y \mathcal{L}_\beta^{xy}(\varphi) + (v_\gamma^y)^2 \mathcal{L}_\beta^{yy}(\varphi).\end{aligned}$$

Applying this to (4.14) gives the following expression

$$\begin{aligned}\mathcal{L}_\gamma^{||} = \frac{15}{8}(-\mathcal{L}_\alpha + \mathcal{L}_\beta) - \frac{7}{16}(v_\gamma^x \mathcal{L}_\alpha^x(\varphi) + v_\gamma^y \mathcal{L}_\alpha^y(\varphi) + v_\gamma^x \mathcal{L}_\beta^x(\varphi) + v_\gamma^y \mathcal{L}_\beta^y(\varphi)) \\ + \frac{1}{32}(-(v_\gamma^x)^2 \mathcal{L}_\alpha^{xx}(\varphi) - 2v_\gamma^x v_\gamma^y \mathcal{L}_\alpha^{xy}(\varphi) - (v_\gamma^y)^2 \mathcal{L}_\alpha^{yy}(\varphi) \\ + (v_\gamma^x)^2 \mathcal{L}_\beta^{xx}(\varphi) + 2v_\gamma^x v_\gamma^y \mathcal{L}_\beta^{xy}(\varphi) + (v_\gamma^y)^2 \mathcal{L}_\beta^{yy}(\varphi)).\end{aligned}$$

Therefore, we have the 24×21 matrix

$$E = \begin{bmatrix} I_{18} & \mathbf{0} \\ \mathbf{0} & L \\ T & \mathbf{0} \end{bmatrix} \quad L = \text{diag}[\ell_1, \ell_2, \ell_3]$$

where the last block (3×18), T, is composed of three sub blocks (3×3, 3×6, and 3×9 respectively)

$$\frac{15}{8}\begin{bmatrix} -1 & 1 & 0 \\ -1 & 0 & 1 \\ 0 & -1 & 1 \end{bmatrix}, \quad -\frac{7}{16}\begin{bmatrix} \mathbf{v}_1^T & \mathbf{v}_1^T & \mathbf{0} \\ \mathbf{v}_2^T & \mathbf{0} & \mathbf{v}_2^T \\ \mathbf{0} & \mathbf{v}_3^2 & \mathbf{v}_3^T \end{bmatrix}, \quad \frac{1}{32}\begin{bmatrix} -\mathbf{w}_1^T & \mathbf{w}_1^T & \mathbf{0} \\ -\mathbf{w}_2^T & \mathbf{0} & \mathbf{w}_2^T \\ \mathbf{0} & -\mathbf{w}_3^2 & \mathbf{w}_3^T \end{bmatrix},$$

where $\mathbf{w}_i^T = \left[(v_i^x)^2, 2v_i^x v_i^y, (v_i^y)^2\right]$.

Finally, notice that by combining (4.10) and (4.13) we get the matrix in (4.8) and

$$C = DE \tag{4.15}$$

4.4.3 Normal Derivatives

During the discussion above we have been concerned with transforming a basis on a local triangle to that of a basis on a reference triangle. However, we have not considered the implications that results from the assumption of always rotating the normal derivative positive $\frac{\pi}{2}$. If we always rotate positive $\frac{\pi}{2}$ there will be a jump discontinuity in the basis function along that edge.

This results from assuming $\frac{\partial \varphi_i}{\partial \mathbf{n}_i} = 1$ on triangle I while at the same time assuming $\frac{\partial \varphi_i}{\partial \mathbf{n}_i} = -1$ on the adjacent triangle J. The issue can be seen graphically in Figure 4.3. This is what causes the discontinuity along shared edges. To address this we need only multiply the value of φ_i by negative one on the triangle J, while leaving φ_i alone on triangle I.

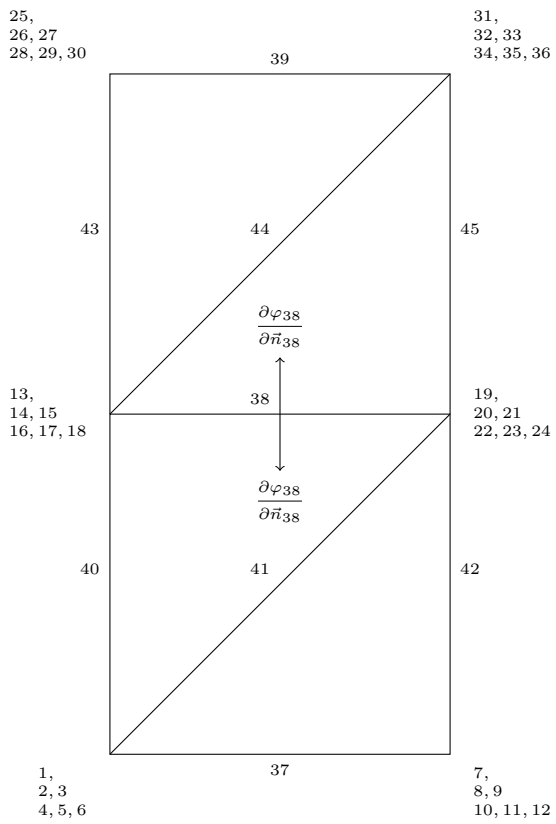

Figure 4.3: Demonstration of Continuity Issue in Normal Derivatives

4.4.4 Interpolation Error

By using Theorem 6.1.1 and inequality (6.1.5) in [8], we obtain the following two approximation properties for the Argyris FEM space X^h:

$$\forall\, \chi \in H^6(\Omega) \cap H_0^2(\Omega),\ \exists\, \chi^h \in X^h \quad \text{such that} \quad \|\chi - \chi^h\|_2 \leq C\, h^4\, |\chi|_6, \tag{4.16}$$

$$\forall\, \chi \in H^4(\Omega) \cap H_0^2(\Omega),\ \exists\, \chi^h \in X^h \quad \text{such that} \quad \|\chi - \chi^h\|_2 \leq C\, h^2\, |\chi|_4, \tag{4.17}$$

$$\forall\, \chi \in H^3(\Omega) \cap H_0^2(\Omega),\ \exists\, \chi^h \in X^h \quad \text{such that} \quad \|\chi - \chi^h\|_2 \leq C\, h\, |\chi|_3, \tag{4.18}$$

where C is a generic constant that can depend on the data, but not on the meshsize h. Approximation property (4.16) follows from inequality (6.1.5) in [8] with $q = 2$, $p = 2$, $m = 2$ and $k+1 = 6$. Approximation property (4.17) follows from inequality (6.1.5) in [8] with $q = 2$, $p = 2$, $m = 2$ and $k+1 = 4$. Approximation property (4.18) follows from inequality (6.1.5) in [8] with $q = 2$, $p = 2$, $m = 2$ and $k+1 = 3$.

4.5 Two Level Method

Although, the streamfunction formulation of the QGE contains only one flow variable, the streamfunction ψ, the streamfunction formulation of the QGE still suffers from having to solve a large nonlinear system of equations. This is usually done by using a nonlinear solver, such as Newton's Method. These nonlinear solvers typically require solving large linear systems multiple times to obtain the solution to the nonlinear system. Solving these large linear systems multiple times can be time consuming. Thus, a two-level algorthm can improve solve times greatly over the standard non-linear sover, since we need only solve the non-linear

system on a coarse mesh and then use that solution to solve a linear system on a fine mesh. To this end, in this section discusses the two-level finite element discretization for the pure streamfunction formulation of the SQGE and QGE in H^2 norm.

4.5.1 Two Level Algorithm

We consider an approximate solution to (3.13) by a two-level finite element procedure as described by [15, 30]. If we let X^h, $X^H \subset H_0^2(\Omega)$ denote two conforming finite element meshes with $H \gg h$. We compute an approximate solution ψ^h in the finite element space X^h by solving a linear system consisting of the degrees of freedom in X^h. This linear system requires us to first compute the approximate solution ψ^H to the nonlinear system in the finite element space X^H where the mesh is very coarse, i.e. $H \gg h$ and then using this solution, ψ^H, in the linear system. This procedure is as follows

Algorithm 1

Step 1: Solve the nonlinear system on a coarse mesh for $\psi^H \in X^H$:

$$a_1(\psi^H, \chi^H) + a_2(\psi^H; \psi^H, \chi^H) + a_3(\psi^H, \chi^H) = \ell(\chi^H), \quad \text{for all } \chi^H \in X^H. \tag{4.19}$$

Step 2: Solve the linear system on a fine mesh for $\psi^h \in X^h$:

$$a_1(\psi^h, \chi^h) + a_2(\psi^H; \psi^h, \chi^h) + a_3(\psi^h, \chi^h) = \ell(\chi^h), \quad \text{for all } \chi^h \in X^h. \tag{4.20}$$

Lemma 4.2. *Given a solution ψ^H of (4.19), then the solution to the following problem exists uniquely*

$$\begin{aligned} &\text{find } \widehat{\psi} \in H_0^2(\Omega) \text{ such that, for all } \chi \in H_0^2(\Omega), \\ &\quad a_1(\widehat{\psi}, \chi) + a_2(\psi^H; \widehat{\psi}, \chi) + a_3(\widehat{\psi}, \chi) = \ell(\chi), \end{aligned} \tag{4.21}$$

and satisfies $\|\widehat{\psi}\|_2 \leq Re\, Ro^{-1} \|F\|_{-2}$.

Proof. First we introduce a new continuous bilinear form $B : H_0^2(\Omega) \times H_0^2(\Omega) \to \mathbb{R}$ given by

$$B(\psi, \chi) = a_1(\psi, \chi) + a_2(\psi^H; \psi, \chi) + a_3(\psi, \chi).$$

B is continuous and coercive and therefore $\widehat{\psi}$ exists and is unique. Now setting $\chi = \widehat{\psi}$ in (4.21) and noting that $a_3(\psi, \chi) = -a_3(\chi, \psi)$ which implies that $a_3(\widehat{\psi}, \widehat{\psi}) = 0$ gives

$$\begin{aligned} Re^{-1} \|\widehat{\psi}\|_2^2 &= \ell(\widehat{\psi}) \\ \|\widehat{\psi}\|_2 &= Re \frac{\ell(\widehat{\psi})}{\|\widehat{\psi}\|_2} \\ &\leq ReRo^{-1} \|F\|_{-2} \|\widehat{\psi}\|_2 \end{aligned}$$

Therefore, it follows that $\|\widehat{\psi}\|_2 \leq Re\, Ro^{-1} \|F\|_{-2}$. □

Lemma 4.3. *The solution to (4.19) exists and satisfies*

$$\|\psi^H\|_2 \leq Re\, Ro^{-1} \|F\|_{-2}.$$

Proof. The bilinear form B is continuous and coercive on X^h and so ψ^h exists and is unique. Setting, $\chi^h = \psi^h$ in (4.20) and again noting that $a_3(\psi^h, \psi^h) = 0$ and using (3.12) gives

$$\begin{aligned} Re^{-1}\|\psi^h\|_2^2 &= \ell(\psi^h) \\ \|\psi^h\|_2 &= Re\frac{\ell(\psi^h)}{\|\psi^h\|_2} \\ &\leq Re\, Ro^{-1}\|F\|_{-2}. \end{aligned}$$

□

4.6 Method of Lines

The *method of lines* refers to the application of the *finite difference* method to a semi-discretization of an equation, i.e. the spatial domain has been discretized by the finite element method and then the time domain is discretized using a finite difference method. This is the preferable method for discretization of the time domain, due to its simplicity and the fact that the time domain does not have geometry.

In particular, we may apply a a *backward Euler* finite difference scheme to (4.1) which would produce the following discretization of the streamfunction form of the QGE

$$a_0(\psi_h^{n+1} - \psi_h^n, \chi_h) + k\,[a_1(\psi_h^n, \chi_h) + a_2(\psi_h^n, \psi_h^n, \chi_h) + a_3(\psi_h^n, \chi_h)] = k\,\ell^n(\chi_h), \quad \forall\, \chi_h \in X^h. \tag{4.22}$$

where k is the time step, subscripts represent the discretization in spatial domains, and superscripts represent the discretization in time domain. Additionally, fince the linear form $\ell(\chi_h)$ is, in fact, time dependent we place a superscript to indicate the discretization of the ℓ in the time domain. The attractiveness of using this backward Euler scheme is that it is explicit and therefore one need not solve the non-linear system that would arize from the *forward Euler* scheme. However, it is well known that the backward Euler scheme is not a-stable and therefore one needs to be careful to satisfy a CFL type condition.

Here in lies the problem with using a high order finite element scheme, such as the Argyris element, and the method of lines; the backward Euler scheme is first order in time whereas the Argyris element is sixth order in the L^2 norm. Thus, we might expect a CFL condition of the form

$$\frac{k}{h^6} \leq C$$

where C is a dimensionless constant that does not depend on either k or h. Thus, we might expect to need quite a small time step, which may be unreasonably small for numerical simulations. Therefore, either a higher order finite difference scheme will need to be used, or an explicit finite difference scheme will need to be employed.

While an implicit scheme might seem an attactive option, one must take into account the ammount of time required to solve the nonlinear system at each time step. For larger spatial discretizations the time to solve such nonlinear systems might be prohibitive. Therefore, higher order finite difference schemes appear to be the more attractive approach.

However, there may be hope for the explicit finite element schemes after all. It might be possible to apply the Two-level method (Algorithm 1) to the QGE at each time step. That is we solve the nonlinear system on a coarse mesh and then use that solution to linearize the nonlinear system on the fine mesh. This method may allow for much quicker calculations than might be expected using just an explicit finite difference scheme alone. We expect that this method will produce good results.

Chapter 5

Error Analysis

5.1 SQGE

The main goal of this section is to develop a rigorous numerical analysis for the FEM discretization of the QGE (4.2) by using the conforming Argyris element. First, in Theorem 5.1 we prove error estimates in the H^2 norm by using an approach similar to that used in [7]. Second, in Theorem 5.4, we prove error estimates in the L^2 and H^1 norms by using a duality argument.

Theorem 5.1. *Let ψ be the solution of* (3.13) *and ψ^h be the solution of* (4.2)*. Furthermore, assume that the following small data condition is satisfied:*

$$Re^{-2}\, Ro \geq \Gamma_1 \|F\|_{-2}, \tag{5.1}$$

where Re is the Reynolds number defined in (2.18)*, Ro is the Rossby number defined in* (2.10)*, Γ_1 is the continuity constant of the trilinear form a_2 in* (3.10)*, and F is the forcing term. Then the following error estimate holds:*

$$|\psi - \psi^h|_2 \leq C(Re, Ro, \Gamma_1, F) \inf_{\chi^h \in X^h} |\psi - \chi^h|_2, \tag{5.2}$$

where

$$C(Re, Ro, \Gamma_1, F) := \left[\frac{Ro^{-1} + 2\, Re^{-1} + \Gamma_1\, Re\, Ro^{-1} \|F\|_{-2}}{Re^{-1} - \Gamma_1\, Re\, Ro^{-1} \|F\|_{-2}} \right] \tag{5.3}$$

is a generic constant that can depend on Re, Ro, Γ_1, F, but not *on the meshsize h.*

Remark 5.2. *Note that the small data condition in Theorem 5.1 involves* both *the Reynolds number and the Rossby number, the latter quantifying the rotation effects in the QGE.*

Furthermore, note that the standard small data condition $Re^{-2} \geq \Gamma_1 \|F\|_{-2}$ used to prove the uniqueness for the steady-state 2D NSE [20, 21, 31] is significantly more restrictive for the QGE, since (5.1) *has the Rossby number (which is small when rotation effects are significant) on the left-hand side. This is somewhat counterintuitive, since in general rotation effects are expected to help in proving the well-posedness of the system. We think that the explanation for this puzzling situation is the following: Rotation effects do make the mathematical analysis of 3D flows more amenable by giving them a 2D character. We, however, are concerned with 2D flows (the QGE). In this case, the small data condition* (5.1) *(needed in proving the uniqueness of the solution) indicates that rotation effects make the mathematical analysis of the (2D) QGE more complicated than that of the 2D NSE.*

Proof. Since $X^h \subset X$, (3.13) holds for all $\chi = \chi^h \in X^h$. Subtracting (4.2) from (3.13) with $\chi = \chi^h \in X^h$ gives

$$\begin{aligned} a_1(\psi - \psi^h, \chi^h) + a_2(\psi, \psi, \chi^h) - a_2(\psi^h, \psi^h, \chi^h) \\ + a_3(\psi - \psi^h, \chi^h) = 0 \qquad \forall \chi^h \in X^h. \end{aligned} \tag{5.4}$$

Next, adding and subtracting $a_2(\psi^h, \psi, \chi^h)$ to (5.4), we get:

$$\begin{aligned} a_1(\psi - \psi^h, \chi^h) + a_2(\psi, \psi, \chi^h) - a_2(\psi^h, \psi, \chi^h) + a_2(\psi^h, \psi, \chi^h) - a_2(\psi^h, \psi^h, \chi^h) \\ + a_3(\psi - \psi^h, \chi^h) = 0 \qquad \forall \chi^h \in X^h. \end{aligned} \tag{5.5}$$

The error e can be decomposed as

$$e := \psi - \psi^h = (\psi - \lambda^h) + (\lambda^h - \psi^h) := \eta + \Phi^h, \tag{5.6}$$

where $\lambda^h \in X^h$ is arbitrary. Thus, equation (5.5) can be rewritten as

$$\begin{aligned} a_1(\eta + \Phi^h, \chi^h) + a_2(\eta + \Phi^h, \psi, \chi^h) + a_2(\psi^h, \eta + \Phi^h, \chi^h) \\ + a_3(\eta + \Phi^h, \chi^h) = 0 \qquad \forall \chi^h \in X^h. \end{aligned} \tag{5.7}$$

Letting $\chi^h := \Phi^h$ in (5.7), we obtain

$$\begin{aligned} a_1(\Phi^h, \Phi^h) + a_3(\Phi^h, \Phi^h) = -a_1(\eta, \Phi^h) - a_2(\eta; \psi, \Phi^h) - a_2(\psi^h; \psi, \Phi^h) \\ - a_2(\psi^h; \eta, \Phi^h) - a_2(\psi^h; \Phi^h, \Phi^h) - a_3(\eta, \Phi^h). \end{aligned} \tag{5.8}$$

Note that, since $a_3(\Phi^h, \Phi^h) = -a_3(\Phi^h, \Phi^h)\ \forall \Phi^h \in X^h \subset X = H_0^2$, it follows that

$$a_3(\Phi^h, \Phi^h) = 0. \tag{5.9}$$

Also, it follows immediately from (3.4) that

$$a_2(\psi^h, \Phi^h, \Phi^h) = 0. \tag{5.10}$$

Combining (5.10), (5.9), and (5.8), we get:

$$\begin{aligned} a_1(\Phi^h, \Phi^h) = -a_1(\eta, \Phi^h) - a_2(\Phi^h; \psi, \Phi^h) - a_2(\eta; \psi, \Phi^h) \\ - a_2(\psi^h; \eta, \Phi^h) - a_3(\eta, \Phi^h). \end{aligned} \tag{5.11}$$

Using

$$a_1(\Phi^h, \Phi^h) = Re^{-1} \left|\Phi^h\right|_2^2$$

and inequalities (3.9) – (3.11) in equation (5.11) gives

$$\begin{aligned} Re^{-1} \left|\Phi^h\right|_2^2 \leq Re^{-1} \left|\eta\right|_2 \left|\Phi^h\right|_2 + \Gamma_1 \Big(\left|\eta\right|_2 \left|\psi\right|_2 \left|\Phi^h\right|_2 + \left|\psi^h\right|_2 \left|\eta\right|_2 \left|\Phi^h\right|_2 \Big) \\ + \Gamma_1 \left|\Phi^h\right|_2^2 \left|\psi\right|_2 + Ro^{-1} \left|\eta\right|_2 \left|\Phi^h\right|_2. \end{aligned} \tag{5.12}$$

Simplifying and rearranging terms in (5.12) gives

$$\left|\Phi^h\right|_2 \leq \left(Re^{-1} - \Gamma_1 \left|\psi\right|_2\right)^{-1} \left(Re^{-1} + \Gamma_1 \left|\psi\right|_2 + \Gamma_1 \left|\psi^h\right|_2 + Ro^{-1}\right) \left|\eta\right|_2. \tag{5.13}$$

Using (5.13) and the triangle inequality along with the stability estimates (3.14) and (4.3) gives

$$\begin{aligned} \left|e\right|_2 &\leq \left|\eta\right|_2 + \left|\Phi^h\right|_2 \\ &\leq \left[1 + \frac{Re^{-1} + \Gamma_1 \left|\psi\right|_2 + \Gamma_1 \left|\psi^h\right|_2 + Ro^{-1}}{Re^{-1} - \Gamma_1 \left|\psi\right|_2}\right] \left|\eta\right|_2 \\ &\leq \left[1 + \frac{Re^{-1} + \Gamma_1 \left(Re\, Ro^{-1} \left\|F\right\|_{-2}\right) + \Gamma_1 \left(Re\, Ro^{-1} \left\|F\right\|_{-2}\right) + Ro^{-1}}{Re^{-1} - \Gamma_1 \left(Re\, Ro^{-1} \left\|F\right\|_{-2}\right)}\right] \left|\eta\right|_2 \\ &= \left[\frac{Ro^{-1} + 2\, Re^{-1} + \Gamma_1\, Re\, Ro^{-1} \left\|F\right\|_{-2}}{Re^{-1} - \Gamma_1\, Re\, Ro^{-1} \left\|F\right\|_{-2}}\right] \left|\psi - \lambda^h\right|_2, \end{aligned} \tag{5.14}$$

where $\lambda^h \in X^h$ is arbitrary. Taking the infimum over $\lambda^h \in X^h$ in (5.14) proves the error estimate (5.2). □

In Theorem 5.1, we proved an error estimate in the H^2 norm. In Theorem 5.4, we will prove error estimates in the L^2 and H^1 norms by using a duality argument. To this end, we first notice that the QGE (2.26) can be written as

$$\mathcal{N}\,\psi = Ro^{-1}\,F, \tag{5.15}$$

where the nonlinear operator $\mathcal{N}$ is defined as

$$\mathcal{N}\,\psi := Re^{-1}\,\Delta^2\psi + J(\psi,\Delta\psi) - Ro^{-1}\,\frac{\partial\psi}{\partial x}. \tag{5.16}$$

The linearization of $\mathcal{N}$ around ψ, a solution of (2.26), yields the following *linear* operator:

$$\mathcal{L}\,\chi := Re^{-1}\,\Delta^2\chi + J(\chi,\Delta\psi) + J(\psi,\Delta\chi) - Ro^{-1}\,\frac{\partial\chi}{\partial x}. \tag{5.17}$$

To find the dual problem associated with the QGE (5.15), we first define the *dual operator* $\mathcal{L}^*$ of $\mathcal{L}$:

$$(\mathcal{L}\,\chi,\psi^*) = (\chi,\mathcal{L}^*\,\psi^*) \qquad \forall\,\psi^* \in X. \tag{5.18}$$

To find $\mathcal{L}^*$, we use the standard procedure: In (5.18), we use the definition of $\mathcal{L}$ given in (5.17) and we "integrate by parts" (i.e., use Green's theorem):

$$\begin{aligned}(\mathcal{L}\,\chi,\psi^*) &= \left(Re^{-1}\,\Delta^2\chi + J(\chi,\Delta\psi) + J(\psi,\Delta\chi) - Ro^{-1}\,\frac{\partial\chi}{\partial x}\,,\,\psi^*\right)\\ &= \left(\chi\,,\,Re^{-1}\,\Delta^2\,\psi^* - J(\psi,\Delta\psi^*) + Ro^{-1}\,\frac{\partial\psi^*}{\partial x}\right) + \Big(J(\chi,\Delta\psi),\psi^*\Big),\end{aligned} \tag{5.19}$$

where to get the first term on the right-hand side of (5.19) we used the skew-symmetry of the trilinear form a_2 in the last two variables and Green's theorem (just as we did in the proof of Theorem 3.1). Next, we apply Green's theorem to the second term on the right-hand side of (5.19):

$$\begin{aligned}\Big(J(\chi,\Delta\psi),\psi^*\Big) &= \chi_x\,\Delta\psi_y\,\psi^* - \chi_y\,\Delta\psi_x\,\psi^*\\ &\overset{Green}{=} -\chi\,\Delta\psi_{yx}\,\psi^* - \chi\,\Delta\psi_y\,\psi^*_x + \chi\,\Delta\psi_{xy}\,\psi^* + \chi\,\Delta\psi_x\,\psi^*_y\\ &= \Big(\chi, J(\Delta\psi,\psi^*)\Big).\end{aligned} \tag{5.20}$$

Equations (5.19)-(5.20) imply:

$$\begin{aligned}(\mathcal{L}\,\chi,\psi^*) &= \left(\chi\,,\,Re^{-1}\,\Delta^2\,\psi^* - J(\psi,\Delta\psi^*) + Ro^{-1}\,\frac{\partial\psi^*}{\partial x}\right) + \Big(\chi, J(\Delta\psi,\psi^*)\Big)\\ &= (\chi,\mathcal{L}^*\,\psi^*).\end{aligned} \tag{5.21}$$

Thus, the *dual operator* $\mathcal{L}^*$ is given by

$$\mathcal{L}^*\,\psi^* = Re^{-1}\,\Delta^2\,\psi^* - J(\psi,\Delta\psi^*) + J(\Delta\psi,\psi^*) + Ro^{-1}\,\frac{\partial\psi^*}{\partial x}. \tag{5.22}$$

For any given $g \in L^2(\Omega)$, the weak formulation of the *dual problem* is:

$$(\mathcal{L}^*\,\psi^*,\chi) = (g,\chi) \qquad \forall\,\chi \in X = H^2_0(\Omega). \tag{5.23}$$

We assume that ψ^*, the solution of (5.23), satisfies the following elliptic regularity estimates:

$$\psi^* \in H^4(\Omega) \cap H^2_0(\Omega), \tag{5.24}$$

$$\|\psi^*\|_4 \le C\,\|g\|_0, \tag{5.25}$$

$$\|\psi^*\|_3 \le C\,\|g\|_{-1}, \tag{5.26}$$

where C is a generic constant that can depend on the data, but not on the meshsize h.

Remark 5.3. *We note that this type of elliptic regularity was also assumed in [7] for the streamfunction formulation of the 2D NSE. In that report, it was also noted that for a polygonal domain satisfying a minimum angle condition, Rannacher et al. [] had actually proved this elliptic regularity.*

The error estimates in the L^2 and H^1 norms that we prove in Theorem 5.4 are derived for the particular space $X^h \subset H_0^2(\Omega)$ consisting of Argyris elements, although the same results can be derived for other conforming C^1 finite element spaces.

Theorem 5.4. *Let ψ be the solution of (3.13) and ψ^h be the solution of (4.2). Assume that the same small data condition as in Theorem 5.1 is satisfied:*

$$Re^{-2}\, Ro \geq \Gamma_1 \left\| F \right\|_{-2}. \tag{5.27}$$

Furthermore, assume that $\psi \in H^6(\Omega) \cap H_0^2(\Omega)$. Then there exist positive constants C_0, C_1 and C_2 that can depend on Re, Ro, Γ_1, F, but not *on the meshsize h, such that*

$$|\psi - \psi^h|_2 \leq C_2\, h^4, \tag{5.28}$$

$$|\psi - \psi^h|_1 \leq C_1\, h^5, \tag{5.29}$$

$$\|\psi - \psi^h\|_0 \leq C_0\, h^6. \tag{5.30}$$

Proof. Estimate (5.28) follows immediately from (4.16) and Theorem 5.1. Estimates (5.30) and (5.29) follow from a duality argument.

The error in the primal problem (3.13) and the interpolation error in the dual problem (5.23) are denoted as

$$e := \psi - \psi^h \qquad e^* := \psi^* - \psi^{*h}, \tag{5.31}$$

respectively.

We start proving the L^2 norm estimate (5.30).

$$\begin{aligned} |e|^2 = (e,e) &= (\mathcal{L}\, e, \psi^*) = (e, \mathcal{L}^*\, \psi^*) \\ &= (e, \mathcal{L}^*\, e^*) + (e, \mathcal{L}^*\, \psi^{*h}) = (\mathcal{L}\, e, e^*) + (\mathcal{L}\, e, \psi^{*h}). \end{aligned} \tag{5.32}$$

The last term on the right-hand side of (5.32) is given by

$$(\mathcal{L}\, e, \psi^{*h}) = \left(Re^{-1}\, \Delta^2 e + J(e, \Delta\, \psi) + J(\psi, \Delta\, e) - Ro^{-1}\, \frac{\partial e}{\partial x}\, ,\, \psi^{*h} \right). \tag{5.33}$$

To estimate this term, we consider the error equation obtained by subtracting (4.2) (with $\psi^h = \psi^{*h}$) from (3.13) (with $\chi = \psi^{*h}$):

$$\left(Re^{-1}\, \Delta^2 e - Ro^{-1}\, \frac{\partial e}{\partial x}\, ,\, \psi^{*h} \right) + \left(J(\psi, \Delta\, \psi) - J(\psi^h, \Delta\, \psi^h)\, ,\, \psi^{*h} \right) = 0. \tag{5.34}$$

Using (5.34), equation (5.33) can be written as follows:

$$(\mathcal{L}\, e, \psi^{*h}) = \left(J(e, \Delta\, \psi) + J(\psi, \Delta\, e) - J(\psi, \Delta\, \psi) + J(\psi^h, \Delta\, \psi^h)\, ,\, \psi^{*h} \right). \tag{5.35}$$

Thus, by using (5.35) equation (5.32) becomes:

$$\begin{aligned} |e|^2 &= (\mathcal{L}\, e, e^*) + (\mathcal{L}\, e, \psi^{*h}) \\ &= Re^{-1}\, (\Delta e, \Delta e^*) - Ro^{-1} \left(\frac{\partial e}{\partial x}, e^* \right) + (J(e, \Delta\psi) + J(\psi, \Delta e), e^*) \\ &+ \left(J(e, \Delta\, \psi) + J(\psi, \Delta\, e) - J(\psi, \Delta\, \psi) + J(\psi^h, \Delta\, \psi^h)\, ,\, \psi^{*h} \right) \\ &= a_1(e, e^*) + a_3(e, e^*) + a_2(e, \psi, e^*) + a_2(\psi, e, e^*) + a_2(e, \psi, \psi^{*h}) \\ &\quad - a_2(\psi, \psi, e^*) + a_2(\psi^h, \psi^h, e^*) \\ &= a_1(e, e^*) + a_3(e, e^*) + a_2(e, \psi, e^*) + a_2(\psi, e, e^*) \\ &\quad - a_2(e, \psi, e^*) + a_2(e, \psi^h, e^*) + a_2(e, e, \psi^*) \end{aligned} \tag{5.36}$$

Using the bounds in (3.9)-(3.11), (5.36) yields:

$$\begin{aligned} |e|^2 &= a_1(e,e^*) + a_3(e,e^*) + a_2(e,\psi,e^*) + a_2(\psi,e,e^*) \\ &\quad -a_2(e,\psi,e^*) + a_2(e,\psi^h,e^*) + a_2(e,e,\psi^*) \\ &\leq Re^{-1}\,|e|_2\,|e^*|_2 + Ro^{-1}\,|e|_2\,|e^*|_2 + \Gamma_1\,|e|_2\,|\psi|_2\,|e^*|_2 + \Gamma_1\,|\psi|_2\,|e|_2\,|e^*|_2 \\ &\quad +\Gamma_1\,|e|_2\,|\psi|_2\,|e^*|_2 + \Gamma_1\,|e|_2\,|\psi^h|_2\,|e^*|_2 + \Gamma_1\,|e|_2\,|e|_2\,|\psi^*|_2 \\ &= |e|_2\,|e^*|_2\,\left(Re^{-1} + Ro^{-1} + \Gamma_1\,|\psi|_2 + \Gamma_1\,|\psi|_2 + \Gamma_1\,|\psi|_2 + \Gamma_1\,|\psi^h|_2\right) \\ &\quad +|e|_2^2\,\left(\Gamma_1\,|\psi^*|_2\right). \end{aligned} \tag{5.37}$$

We start bounding the terms on the right-hand side of (5.37). First, we note that using the stability estimates (3.14) for ψ and (4.3) for ψ^h, the right-hand side of (5.37) can be bounded as follows:

$$|e|^2 \leq C\,|e|_2\,|e^*|_2 + |e|_2^2\,\left(\Gamma_1\,|\psi^*|_2\right), \tag{5.38}$$

where C is a generic constant that can depend on Re, Ro, Γ_1, F, but *not* on the meshsize h. By using the approximation results (4.17), we get:

$$|e^*|_2 \leq C\,h^2\,|\psi^*|_4. \tag{5.39}$$

By using (5.24) and (5.25), the elliptic regularity results of the dual problem (5.23) with $g := e$, we also get:

$$|\psi^*|_4 \leq C\,|e|, \tag{5.40}$$

which obviously implies

$$|\psi^*|_2 \leq C\,|e|. \tag{5.41}$$

Inequalities (5.39)-(5.40) imply:

$$|e^*|_2 \leq C\,h^2\,|e|. \tag{5.42}$$

Inserting (5.41) and (5.42) in (5.38), we get:

$$|e|^2 \leq C\,h^2\,|e|_2\,|e| + C\,|e|_2^2\,|e|. \tag{5.43}$$

Using the obvious simplifications and the H^2 error estimate (5.28) in (5.43) yields:

$$|e| \leq C\,h^2\,|e|_2 + C\,|e|_2^2 \leq C\,h^6 + C\,h^8 = C_0\,h^6, \tag{5.44}$$

which proves the L^2 error estimate (5.30).

Next, we prove the H^1 norm estimate (5.29). Since the duality approach we use is similar to that we used in proving the L^2 norm estimate (5.30), we only highlight the main differences. We start again by writing the H^1 norm of the error in terms of the dual operator $\mathcal{L}^*$:

$$\begin{aligned} |e|_1^2 &= (\nabla e, \nabla e) = (e, -\Delta e) = (\mathcal{L}\,e, \psi^*) = (e, \mathcal{L}^*\,\psi^*) \\ &= (e, \mathcal{L}^*\,e^*) + (e, \mathcal{L}^*\,\psi^{*h}) = (\mathcal{L}\,e, e^*) + (\mathcal{L}\,e, \psi^{*h}). \end{aligned} \tag{5.45}$$

Thus, the second and fourth equalities in (5.45) clearly indicate that in the dual problem (5.23), one should choose $g = -\Delta e$, and not $g = e$, as we did in (5.40), when we proved the L^2 error estimate (5.30). Using (5.24) and (5.26), the elliptic regularity results of the dual problem (5.23) with $g := -\Delta e$, we also get:

$$|\psi^*|_3 \leq C\,|-\Delta e|_{-1} \leq C\,|e|_1, \tag{5.46}$$

where in the last inequality we used the fact that $e \in H_0^2(\Omega)$. Inequality (5.46) obviously implies

$$|\psi^*|_2 \leq C\,|e|_1. \tag{5.47}$$

All the results in (5.33)-(5.37) carry over to our setting. Thus, we get:

$$|e|_1^2 \leq C\,|e|_2\,|e^*|_2 + C\,|e|_2^2\,|\psi^*|_2, \tag{5.48}$$

where C is a generic constant that can depend on Re, Ro, Γ_1, F, but *not* on the meshsize h. By using the approximation result (4.18), we get:

$$|e^*|_2 \leq C\,h\,|\psi^*|_3. \tag{5.49}$$

Inequalities (5.49)-(5.46) imply:

$$|e^*|_2 \leq C\,h\,|e|_1. \tag{5.50}$$

Inserting (5.47) and (5.50) in (5.48), we get:

$$|e|_1^2 \leq C\,h\,|e|_2\,|e|_1 + C\,|e|_2^2\,|e|_1. \tag{5.51}$$

Using the obvious simplifications and the H^2 error estimate (5.28) in (5.51) yields:

$$|e|_1 \leq C\,h\,|e|_2 + C\,|e|_2^2 \leq C\,h^5 + C\,h^8 = C_1\,h^5, \tag{5.52}$$

which proves the H^1 error estimate (5.29). □

5.1.1 Two Level Method

The main goal of this section is to develop a rigorous numerical analysis for Algorithm 1. The proof for the error bounds follows a very similar pattern presented in [15].

To this end, we first introduce an improved bound on the trilinear form $a_2(\zeta;\xi,\chi)$ using the discrete Sobolev inequality, i.e.

$$\|\nabla\varphi^h\|_{L^\infty} \leq c\sqrt{|\ln(h)|}\cdot|\varphi^h|_2.$$

The following lemma follows from the above inequality and (3.10)

Lemma 5.5. *For any $\chi^h \in X^h$, the following inequalities hold*

$$|a_2(\psi;\chi^h,\xi)| \leq C\sqrt{|\ln(h)|}\cdot|\psi|_2|\xi|_1|\chi^h|_2,$$
$$|a_2(\psi;\xi,\chi^h)| \leq C\sqrt{|\ln(h)|}\cdot|\psi|_2|\xi|_1|\chi^h|_2.$$

The following lemma will prove useful for proving the error bounds for Algorithm 1

Lemma 5.6. *For ψ, ξ, $\chi \in H_0^2(\Omega)$, we have*

$$a_2(\psi;\xi,\chi) = a_2^*(\xi;\chi,\psi) - a_2^*(\chi;\xi,\psi) \tag{5.53}$$

where

$$a_2^*(\xi;\chi,\psi) = \int_\Omega(\chi_y\xi_{xy} - \xi_x\chi_{yy})\psi_y - (\xi_y\chi_{yx} - \xi_y\chi_{xx})\psi_x\,d\vec{x}. \tag{5.54}$$

For a proof see [15].

The following theorem gives the error bound after Step 2 and is the main result of this paper. The proof of this theorem is similar to the proof for a similar theorem in [15].

Theorem 5.7. *Let X^h, $X^H \in H_0^2(\Omega)$ be two finite element spaces. Let ψ be the solution to* (3.13) *and ψ^h the solution to* (4.20)*. Then ψ^h satisfies*

$$|\psi - \psi^h|_2 \leq C_1 \inf_{\lambda^h\in X^h}|\psi - \lambda^h|_2 + C_2\sqrt{|\ln h|}\cdot|\psi - \psi^H|_1 \tag{5.55}$$

where $C_1 = 2 + Re\,Ro^{-1} + Re^2Ro^{-1}\Gamma_1\|F\|_{-2}$ and $C_2 = 2Re^2Ro^{-1}\Gamma_1 C\,\|F\|_{-2}$.

Proof. Subtracting (4.20) from (3.13) and letting $\chi = \chi^h$ yields

$$a_1(\psi - \psi^h, \chi^h) + a_2(\psi; \psi, \chi^h) - a_2(\psi^H; \psi^h, \chi^h) + a_3(\psi - \psi^h, \chi^h) = 0, \quad \forall \chi^h \in X^h.$$

Using Proposition 5.6 gives

$$\begin{aligned} a_1(\psi - \psi^h, \chi^h) + a_2^*(\psi; \chi^h, \psi) - a_2^*(\chi^h; \psi, \psi) \\ -a_2^*(\psi^h; \chi^h, \psi^H) + a_2^*(\chi^h; \psi^h, \psi^H) + a_3(\psi - \psi^h, \chi^h) = 0, \quad \forall \chi^h \in X^h. \end{aligned}$$

Now, adding the terms

$$-a_2^*(\psi^h; \chi^h, \psi) + a_2^*(\chi^h; \psi^h, \psi) + a_2^*(\psi^h; \chi^h, \psi) - a_2^*(\chi^h; \psi^h, \psi)$$

gives

$$\begin{aligned} &a_1(\psi - \psi^h, \chi^h) + a_2^*(\psi - \psi^h; \chi^h, \psi) + a_2^*(\chi^h; \psi^h - \psi, \psi) \\ &\quad + a_2^*(\psi^h; \chi^h, \psi - \psi^H) + a_2^*(\chi^h; \psi^h, \psi^H - \psi) + a_3(\psi - \psi^h, \chi^h) = 0, \quad \forall \chi^h \in X^h. \end{aligned}$$

Take $\lambda^h \in H_0^2(\Omega)$ arbitrary and define $e := \psi - \psi^h = \eta - \Phi^h$ where $\Phi^h = \psi^h - \lambda^h$ and $\eta = \psi - \lambda^h$ and we have

$$\begin{aligned} &a_1(\Phi^h, \chi^h) + a_2^*(\Phi^h; \chi^h, \psi) - a_2^*(\chi^h; \Phi^h, \psi) + a_3(\Phi^h, \chi^h) \\ &\quad = a_1(\eta, \chi^h) + a_2^*(\eta; \chi^h, \psi) - a_2^*(\chi^h; \eta, \psi) \\ &\quad + a_2^*(\psi^h; \chi^h, \psi - \psi^H) + a_2^*(\chi^h; \psi^h, \psi^H - \psi) + a_3(\eta, \chi^h), \quad \forall \chi^h \in X^h. \end{aligned}$$

Since this holds for any $\chi^h \in H_0^2(\Omega)$ it holds in particular for $\chi^h = \Phi^h \in H_0^2(\Omega)$ which implies

$$\begin{aligned} a_1(\Phi^h, \Phi^h) + a_3(\Phi^h, \Phi^h) = a_1(\eta, \Phi^h) + a_2^*(\eta; \Phi^h, \psi) - a_2^*(\Phi^h; \eta, \psi) \\ + a_2^*(\psi^h; \Phi^h, \psi - \psi^H) + a_2^*(\Phi^h; \psi^h, \psi^H - \psi) + a_3(\eta, \Phi^h). \end{aligned}$$

Note that $a_3(\psi, \chi) = -a_3(\chi, \psi)$ and so it follows that $a_3(\Phi^h, \Phi^h) = 0$. This combined with Proposition 5.6 implies

$$\begin{aligned} a_1(\Phi^h, \Phi^h) = a_1(\eta, \Phi^h) + a_2(\psi; \eta, \Phi^h) \\ + a_2^*(\psi^h; \Phi^h, \psi - \psi^H) + a_2^*(\Phi^h; \psi^h, \psi^H - \psi) + a_3(\eta, \Phi^h). \end{aligned}$$

Using the error bounds given in (3.9), (3.10), (3.11), (3.12), Proposition 5.5, Proposition 3.1, Proposition 4.1 and Proposition 4.2 gives

$$\begin{aligned} Re^{-1}|\Phi^h|_2^2 &\leq Re^{-1}|\eta|_2 \, |\Phi^h|_2 + \Gamma_1 \, |\psi|_2 \, |\eta|_2 \, |\Phi^h|_2 \\ &\quad + 2\Gamma_1 \, C \, |\psi^H|_2 \, |\Phi^h|_2 \, |\psi - \psi^H|_1 \sqrt{|\ln(h)|} + Ro^{-1}|\eta|_2 \, |\Phi^h|_2 \\ &= \left(Ro^{-1} + Re^{-1} + \Gamma_1 \, |\psi|_2\right) |\eta|_2 \, |\Phi^h|_2 + 2\Gamma_1 \, C \, |\psi^H|_2 \, |\Phi^h|_2 |\psi - \psi^H|_1 \sqrt{|\ln(h)|} \\ |\Phi^h|_2 &\leq \left(1 + Re \, Ro^{-1} + Re^2 Ro^{-1} \Gamma_1 \, \|F\|_{-2}\right) |\eta|_2 \\ &\quad + 2Re^2 Ro^{-1} \Gamma_1 \, C \, \|F\|_{-2} \, |\psi - \psi^H|_1 \sqrt{|\ln(h)|} \end{aligned}$$

Adding $|\eta|_2$ to both sides and using the triangle inequality ($|\psi - \psi^h|_2 \leq |\Phi^h|_2 + |\eta|_2$) gives

$$\begin{aligned} |\Phi^h|_2 \leq \left(2 + Re \, Ro^{-1} + Re^2 Ro^{-1} \Gamma_1 \, \|F\|_{-2}\right) |\eta|_2 \\ + 2Re^2 Ro^{-1} \Gamma_1 \, C \, \|F\|_{-2} \, |\psi - \psi^H|_1 \sqrt{|\ln(h)|} \end{aligned}$$

Thus, we have the following estimate for the error bounds

$$|\psi - \psi^h|_2 \leq C_1 \inf_{\lambda^h \in X^h} |\psi - \lambda^h|_2 + C_2 \sqrt{|\ln h|} \cdot |\psi - \psi^H|_1$$

where $C_1 = 2 + Re \, Ro^{-1} + Re^2 Ro^{-1} \Gamma_1 \|F\|_{-2}$ and $C_2 = 2Re^2 Ro^{-1} \Gamma_1 C \, \|F\|_{-2}$. □

As an example, consider the case of the Argyris triangle; for this element we have the following inequalities for this particular element the following theorem follows from approximation theory [3] and Theorem 6.1.1 [8]:

$$|\psi - \psi^h|_j \leq Ch^{6-j}$$
$$|\psi - \psi^H|_j \leq CH^{6-j}$$

Corollary 5.8. *Let X^h, $X^H \in H_0^2(\Omega)$ be the Argyris finite elements, then ψ^h satisfies*

$$|\psi - \psi^h|_2 \leq C_1 h^4 + C_2\sqrt{|\ln(h)|} \cdot H^5. \tag{5.56}$$

Proof. This follows directly by substituting the inequalities for the Argyris triangle bounds into (5.55). □

5.2 QGE

In this section the finite error analysis for the QGE will be presented. We will rely heavily on the previous section containing the finite error analysis for the SQGE (Section 5.1).

5.3 LES

In this section an error analysis of the Filtered QGE associated with the finite element discretization will be explored. The analysis will be similar to the analysis already done in Section 5.1, except we will have to pay special attention to the closure model and its associated error.

Chapter 6

Numerical Tests

6.1 SQGE

The main goal of this section is twofold. First, we show that the FE discretization of the streamfunction formulation of the SQGE (2.28) with the Argyris element produces accurate numerical approximations. To this end, we benchmark our numerical results against those in the published literature [48, 6, 39]. The second goal is to show that the numerical results follow the theoretical error estimates in Proposition 5.1 and Proposition 5.4, i.e., we compare the observed rates of convergence to the theoretical rates of convergence developed in Section 5.1.

Although the pure streamfunction formulation of the steady SQGE (2.28) is our main concern, we also test our Argyris FE discretization on two simplified settings: (i) the *Linear Stommel* model; and (ii) *Linear Stommel-Munk* model. The reason for using these two additional numerical tests is that they are standard test problems in the geophysical fluid dynamics literature (see, e.g., Chapter 13 in Vallis [48] as well as the reports of Myers *et al.* [39], and Cascon *et al.* [6]). This allows us to benchmark our numerical results against those in the published literature. Since both the Linear Stommel and the Linear Stommel-Munk models lack the nonlinearity present in the SQGE (2.28), the represent good stepping stones to verifying our FE discretization.

The *Linear Stommel-Munk* model (see p. 587 in [48] and problem 2 in [6]) is given by

$$\epsilon_s \Delta\psi - \epsilon_m \Delta^2 \psi + \frac{\partial \psi}{\partial x} = f, \tag{6.1}$$

where ϵ_s and ϵ_m are the Stommel Number and Munk Scale, respectively. The Stommel Number and Munk Scale are given by (Equation 10 in [39])

$$\epsilon_m = \frac{A}{\beta L^3} \qquad \epsilon_s = \frac{\gamma}{\beta L}$$

where A, β, L, and γ are the eddy visosity, the β-plane effect, characteristic length scale, and the bottom friction decay rate, respectively. The model is supplemented with appropriate boundary conditions, which will be described for each of the subsequent numerical tests.

We note that the Linear Stommel-Munk model (6.1) is similar in form to the SQGE (2.28). Indeed, both models contain the biharmonic operator $\Delta^2\psi$, the rotation term $\dfrac{\partial \psi}{\partial x}$, and the forcing term F. The two main differences between the two models are the following: First, the SQGE are nonlinear, since they contain the Jacobian term $J(\psi, q)$; the Stommel-Munk model is linear, since it doesn't contain the Jacobian term. The second difference is that the Linear Stommel-Munk model contains a Laplacian term $\Delta\psi$, whereas the SQGE does not.

We also note that the two models use different parameters: the Reynolds number Re and the Rossby number Ro in (2.28) and the Stommel number ϵ_s and the Munk scale ϵ_m in the Linear Stommel-Munk

model. These two sets of parameters, however, are related by the following relations:

$$\epsilon_m = Ro\, Re^{-1} \tag{6.2}$$

$$\epsilon_s = Ro\frac{\gamma L}{U} \tag{6.3}$$

$$\tag{6.4}$$

The second simplified model used in our numerical investigation is the *Linear Stommel* model (Equation 14.22 in [48] and Equation 11 in [39])

$$\epsilon_s \Delta\psi + \frac{\partial\psi}{\partial x} = f. \tag{6.5}$$

We note that the Linear Stommel Model (6.5) is just the Linear Stommel-Munk model (6.1) in which the biharmonic term is dropped (i.e. $\epsilon_m = 0$).

The rest of the subsection is organized as follows: In Subsection 6.1.1 we present results for the Linear Stommel model (6.5). In Subsection 6.1.2 we present results for the Linear Stommel-Munk model (6.1). Finally, in Subsection 6.1.3 we present results for the nonlinear SQGE (2.28).

6.1.1 Linear Stommel Model

This subsection presents the results for the FE discretization of the Linear Stommel model (6.5) by using the Argyris element. The computational domain is $\Omega = [0,1] \times [0,1]$. For completeness, we present results for two numerical tests. The first test, denoted by Test 1, corresponds to the exact solution used by Vallis (Equation 14.38 in [48]), while the second test, denoted by Test 2, corresponds to the exact solution used by Myers *et al.* (Equations 15 and 16 in [39]).

Test 1a: In this test, we choose the same setting as that used by Vallis (Equation 14.38 in [48]). In particular, the forcing term and the non-homogeneous Dirichlet boundary conditions are chosen to match those given by the exact solution

$$\psi(x,y) = (1 - x - e^{-x/\epsilon_s}) \sin \pi y \tag{6.6}$$

We choose the same Stommel number as that used by Vallis, i.e. $\epsilon_s = 0.04$. The exact solution (6.6) considered by Vallis satisfies $\psi \to 0$ as $x \to 0$, but does not vanish at $x = 1$. In our numerical tests, we used a standard lifting procedure to treat these non-homogeneous boundary conditions, i.e. for a problem of the form

$$\begin{aligned} L\psi &= f \text{ on } \Omega \\ \psi &= g \text{ on } \partial\Omega, \end{aligned}$$

we reformulate it to be

$$\begin{aligned} L\widetilde{\psi} &= \widetilde{f} \text{ on } \Omega \\ \widetilde{\psi} &= 0 \text{ on } \partial\Omega \end{aligned}$$

where $L\widetilde{\psi} = Lu - LS = f - g = \widetilde{f}$ and the solution ψ from the original problem can then be found by $\psi(x,y) = \widetilde{\psi} + S$. The function $S(x,y)$ is assumed to have the form

$$S(x,y) = A(y)(1-x) + B(y)x$$

and satisfies the boundary conditions given by (6.7). After some simple algebra we see that

$$S(x,y) = -xe^{-x/\epsilon_s}\pi \sin(\pi y).$$

The function $\widetilde{f}$ can be determined by applying the operator L corresponding to the *Linear Stommel* problem to $u - S$

Applying the finite element method to the *Linear Stommel* problem with the new modified $\widetilde{f}$, corresponding to the exact solution given by Vallis, and homogeneous boundary conditions using Argyris Finite

Elements we get a solution that matches the solution presented by Vallis, as can be seen in Figure 6.1. Additionally, the table of errors Table 6.1 shows the order of convergence appears to be approaching the expected rates for $L^2, H^1,$ and H^2 norms. Figure 6.1 presents the streamlines of the approximate solution obtained by using the Argyris Finite Element on a mesh with $h = \frac{1}{32}$ and 9670 DoFs. Comparing Figure 6.1 with Figure 14.5 in [48], we notice that our approximation is close to his. Since the exact solution is available, we can compute the errors in various norms. Table 6.1 presents the errors e_0, e_1, and e_2 (i.e., the L^2, H^1, and H^2 errors, respectively) for various values of the mesh sizes, h (the DoFs are also included).

h	$DoFs$	e_0	L_2 order	e_1	H^1 order	e_2	H^2 order
$1/2$	70	0.1148	–	1.81	–	83.67	–
$1/4$	206	0.01018	3.495	0.312	2.537	25.48	1.716
$1/8$	694	0.0004461	4.512	0.02585	3.593	3.902	2.707
$1/16$	2534	1.09×19^{-5}	5.355	0.001215	4.412	0.3494	3.481
$1/32$	9670	1.972×19^{-7}	5.788	4.349×19^{-5}	4.804	0.02335	3.903

Table 6.1: Errors and Rate of Convergence for the Linear Stommel Model (6.5), Test 1 [48]

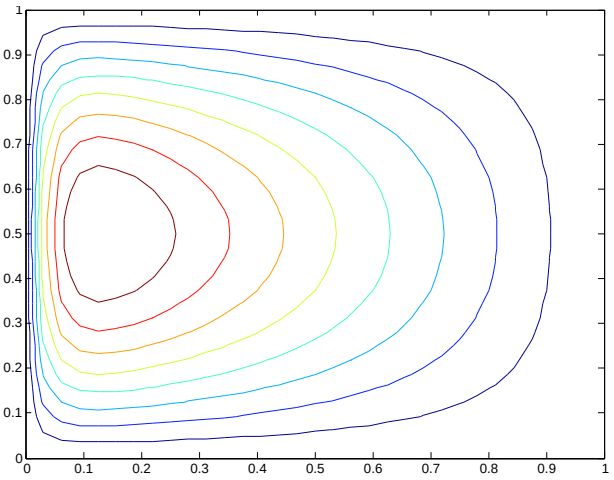

Figure 6.1: Linear Stommel Model (6.5), Test 1a [48]: Streamlines of the approximation, ψ^h, $h = \frac{1}{32}$, and 9670 DoFs.

We note that the errors in Table 6.1 follow the theoretical rates of convergence predicted by the estimates (5.28) - (5.30) in Proposition 5.4. The orders of convergence in Table 6.1 are close to the theoretical ones for the fine meshes, but not as close for the coarse meshes. We think that the inaccuracies on the coarse meshes are due to their inability to capture the thin boundary layer on the left-hand side (i.e., at $x = 0$). The finer the mesh gets, the better this boundary layer is captured and the better the numerical accuracy becomes.

Test 1b: In the Second part of Test 1, we verify the hypothesis above, that is, whether the degrading accuracy of the approximation is indeed due to the thin western boundary layer. To this end, we change the Stommel number in Test 1a to be $\epsilon_s = 1$, which will result in a much thicker western boundary layer. We then run the same numerical test as before, but with the new Stommel number. As can be seen in Table 6.2, the rates of convergence are the expected theoretical orders of convergence. This shows that the reason for the inaccuracies in Table 6.1 were indeed due to the thin western boundary layer.

h	$DoFs$	e_0	L_2 order	e_1	H^1 order	e_2	H^2 order
$1/2$	70	1.689×10^{-5}	–	0.0003434	–	0.008721	–
$1/4$	206	3.722×10^{-7}	5.504	1.341×10^{-5}	4.678	0.0005616	3.957
$1/8$	694	4.891×10^{-9}	6.25	3.757×10^{-7}	5.158	3.25×10^{-5}	4.111
$1/16$	2534	7.079×10^{-11}	6.111	1.117×10^{-8}	5.071	1.964×10^{-6}	4.049
$1/32$	9670	1.08×10^{-12}	6.035	3.437×10^{-10}	5.023	1.213×10^{-7}	4.018

Table 6.2: Errors and Rate of Convergence for the Linear Stommel Model (6.5), Test 1b [48]

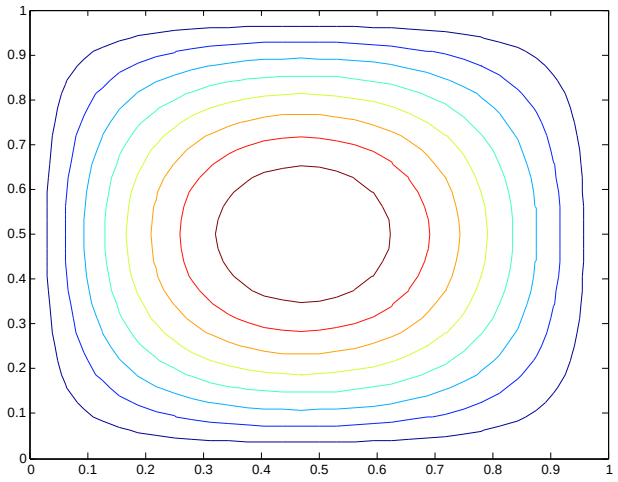

Figure 6.2: Linear Stommel Model (6.5), Test 1b [48]: Streamlines of the approximation, ψ^h, $h = \frac{1}{32}$, and 9670 DoFs with $\epsilon_s = 1$.

Test 2: For our second test we use the exact solution given by Myers (Equations 15 and 16 in [39]), i.e.

$$\psi(x,y) = \frac{\sin(\pi y)}{\pi(1+4\pi^2\epsilon_s^2)}\left\{2\pi\epsilon_s \sin(\pi x) + cos(\pi x) + \frac{1}{e^{R_1} - e^{R_2}}\left[(1+e^{R_2})e^{R_1 x} - (1+e^{R_1})e^{R_2 x}\right]\right\}, \tag{6.7}$$

where R_1 and R_2 are the positive and negative roots, respectively, of

$$R = \frac{-1 \pm \sqrt{1+4\pi^2\epsilon_s^2}}{2\epsilon_s}.$$

The forcing term and the homogeneous Dirichlet boundary conditions are chosen to match those given by the exact solution (6.7). We choose the same Stommel number as that used by Myers, i.e. $\epsilon_s = 0.05$.

Figure 6.3 presents the streamlines of the approximate solution obtained by using the Argyris Finite Element on a mesh with $h = \frac{1}{32}$ and 9670 DoFs. Comparing Figure 6.3 with Figure 2 in [39], we notice that our approximation is close to that in [39]. Since the exact solution is available, we can compute the errors in various norms. Table 6.3 presents the errors e_0, e_1, and e_2 (i.e., the L^2, H^1, and H^2 errors, respectively) for various values of the mesh sizes, h.

h	$DoFs$	e_0	L_2 order	e_1	H^1 order	e_2	H^2 order
$1/2$	70	0.005645	–	0.1451	–	6.602	–
$1/4$	206	0.0004276	3.723	0.02081	2.801	1.632	2.016
$1/8$	694	1.46×10^{-5}	4.872	0.001408	3.886	0.2066	2.982
$1/16$	2534	2.954×10^{-7}	5.627	5.829×10^{-5}	4.594	0.0165	3.646
$1/32$	9670	4.968×10^{-9}	5.894	1.998×10^{-6}	4.867	0.001069	3.948

Table 6.3: Errors and Rate of Convergence for the Linear Stommel Model (6.5), Test 2 [39]

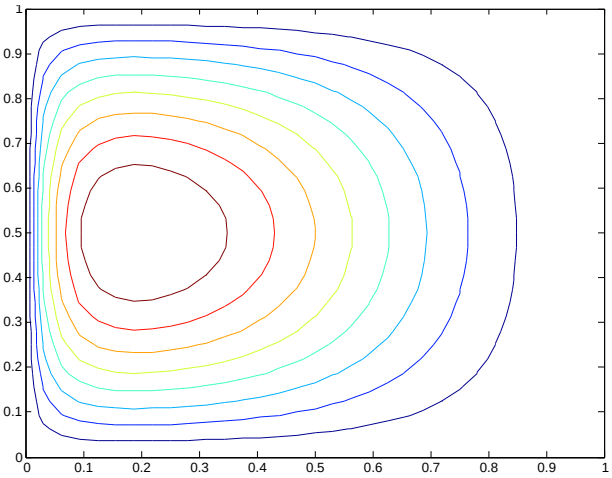

Figure 6.3: Linear Stommel Model (6.5), Test 2 [39]: Streamlines of the approximation, ψ^h, $h = \frac{1}{32}$, and 9670 DoFs.

We note that the errors in Table 6.3 follow the theoretical rates of convergence predicted by the estimates (5.28) - (5.30) in Proposition 5.4. Again, we see that the orders of convergence in Table 6.3 are close to the theoretical ones for the fine meshes, but not as close for the coarse meshes. We attribute this to the inaccuracies at the thin boundary layer on the left-hand side (i.e., at $x = 0$). The finer the mesh gets, the better this boundary layer is captured and the better the numerical accuracy becomes.

6.1.2 Linear Stommel-Munk Model

This subsection presents results for the FE discretization of the Linear Stommel-Munk model (6.1) by using the Argyris element. Our computational setting is the same as taht used by Cascon *et al.* [6]: The computational domain is $\Omega = [0, 3] \times [0, 1]$, the Munk scale is $\epsilon_m = 6 \times 10^{-5}$, the Stommel number is $\epsilon_s = 0.05$, and the boundary conditions are

$$\psi = \frac{\partial \psi}{\partial \mathbf{n}} = 0 \quad \text{on } \partial\Omega \tag{6.8}$$

For completeness, we present results for two numerical tests, denoted by Test 3 and Test 4, both corresponding to Test 1 and Test 2 in [6], respectively.

Test 3: For our third test we use the exact solution given by Test 1 in [6], i.e.

$$\psi(x, y) = \sin^2 \frac{\pi x}{3} \sin^2 \pi y. \tag{6.9}$$

The forcing term is chosen to match that given by the exact solution (6.9).

For this third test we take F corresponding to applying the linear operator L associated with the *Linear Stommel-Munk* model to the exact solution (6.9).

Figure 6.4 presents the streamlines of the approximate solution obtained by using the Argyris Finite Element on a mesh with $h = \frac{1}{32}$ and 28550 DoFs. Comparing Figure 6.4 with Figure 7 in [39], we notice that our approximation is close to that in [39]. Since the exact solution is available, we can compute the errors in various norms. Table 6.4 presents the errors e_0, e_1, and e_2 (i.e., the L^2, H^1, and H^2 errors, respectively) for various values of the mesh sizes, h.

h	$DoFs$	e_0	L_2 order	e_1	H^1 order	e_2	H^2 order
$1/2$	170	0.00299	–	0.04084	–	0.7624	–
$1/4$	550	3.217×10^{-5}	6.539	0.001031	5.308	0.04078	4.225
$1/8$	1958	3.437×10^{-7}	6.548	2.491×10^{-5}	5.371	0.002253	4.178
$1/16$	7366	4.571×10^{-9}	6.232	7.026×10^{-7}	5.148	0.0001344	4.067
$1/32$	28550	6.704×10^{-11}	6.091	2.113×10^{-8}	5.056	8.26×10^{-6}	4.024

Table 6.4: Errors and Rate of Convergence for the Linear Stommel-Munk Model (6.8), Test 3 [6]

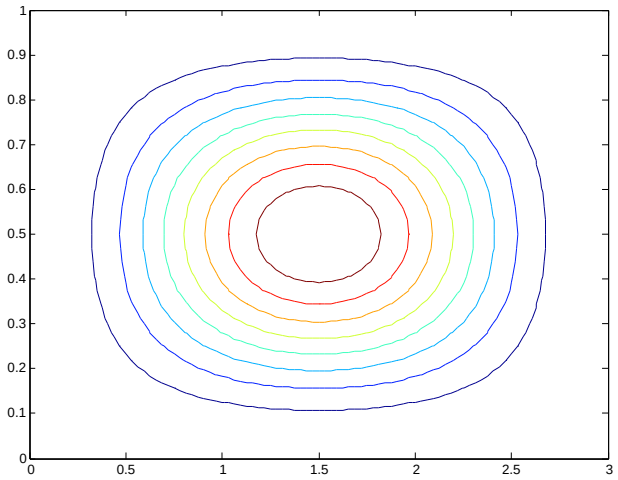

Figure 6.4: Linear Stommel-Munk Model (6.8), Test 3 [6]: Streamlines of the approximation, ψ^h, on a mesh size, $h = \frac{1}{32}$, and 28550 DoFs.

We note that the errors in Table 6.4 follow the theoretical rates of convergence predicted by the estimates (5.28) - (5.30) in Proposition 5.4. This time, we see that the orders of convergence in Table 6.4 are close to the theoretical ones for the fine meshes, but are higher than expected for the for the coarse meshes. We attribute this to the fact that the exact solution (6.9) does not display any boundary layers that could be challenging to capture by the Argyris element on a coarse mesh.

Test 4: For our fourth test we use the exact solution given by Test 2 in [6], i.e.

$$\psi(x, y) = \left[\left(1 - \frac{x}{3}\right)\left(1 - e^{-20x}\right)\sin \pi y\right]^2. \tag{6.10}$$

Again we take the forcing term F corresponding the exact solution (6.10).

Figure 6.5 presents the streamlines of the approximate solution obtained by using the Argyris Finite Element on a mesh with $h = \frac{1}{32}$ and 28550 DoFs. Comparing Figure 6.5 with Figure 10 in [39], we notice

that our approximation is close to [39]. Since the exact solution is available, we can compute the errors in various norms. Table 6.5 presents the errors e_0, e_1, and e_2 (i.e., the L^2, H^1, and H^2 errors, respectively) for various values of the mesh sizes, h.

h	$DoFs$	e_0	L_2 order	e_1	H^1 order	e_2	H^2 order
$1/2$	170	0.06036	–	1.162	–	38.99	–
$1/4$	550	0.01132	2.414	0.3995	1.541	21.4	0.8656
$1/8$	1958	0.0008399	3.753	0.05914	2.756	5.656	1.92
$1/16$	7366	2.817×10^{-5}	4.898	0.004008	3.883	0.7378	2.939
$1/32$	28550	5.587×10^{-7}	5.656	0.0001607	4.641	0.0597	3.627

Table 6.5: Errors and Rate of Convergence for the Linear Stommel-Munk Model (6.8), Test 4 [6]

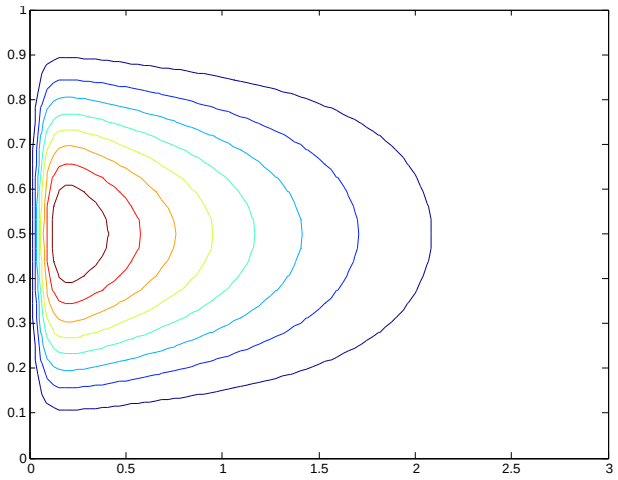

Figure 6.5: Linear Stommel-Munk Model (6.8), Test 4 [6]: Streamlines of the approximation, ψ^h, $h = \frac{1}{32}$, and 28550 DoFs.

We note that the errors in Table 6.5 follow the theoretical rates of convergence predicted by the estimates (5.28) - (5.30) in Proposition 5.4. Again, we see that the orders of convergence in Table 6.5 are close to the theoretical ones for the fine meshes, but not as close for the coarse meshes. As stated previously, we attribute this to the inaccuracies at the thin boundary layer on the left-hand side (i.e., at $x = 0$). The finer the mesh gets, the better this boundary layer is captured and the better the numerical accuracy becomes.

6.1.3 Stationary Quasigeostrophic Equations

This subsection presents results for the FE discretization of the streamfunction formulation of the SQGE (2.28) by using the Argyris element. Our computational domain is $\Omega = [0, 3] \times [0, 1]$, the Reynolds number is $Re = 1.667$, and the Rossby number is $Ro = 10^{-4}$. For completeness, we present results for two numerical tests, denoted by Test 5 and Test 6, both corresponding to the exact solutions given in Test 1 and Test 2 of [6], respectively.

Test 5: In this test, we take the same exact solution presented in *Test 3*, i.e.

$$\psi(x, y) = \sin^2 \frac{\pi x}{3} \cdot \sin^2 \pi y. \tag{6.11}$$

Again, the forcing term F and homogeneous boundary conditions, $\psi = \frac{\partial \psi}{\partial \mathbf{n}} = 0$, correspond to the exact solution (6.11).

Table 6.1.3 presents the streamlines of the approximate solution obtained by using the Argyris Finite Element on a mesh with $h = \frac{1}{32}$ and 28550 DoFs. We note that the streamlines look as we expect and are similar to those given by Figure 7 in [39], which uses the same exact solution. Since the exact solution is available, we can compute the errors in various norms. Table 6.6 presents the errors e_0, e_1, and e_2 (i.e., the L^2, H^1, and H^2 errors, respectively) for various values of the mesh sizes, h.

h	$DoFs$	e_0	L_2 order	e_1	H^1 order	e_2	H^2 order
$1/2$	170	0.005709	–	0.06033	–	1.087	–
$1/4$	550	3.726×10^{-5}	7.259	0.001086	5.796	0.04113	4.724
$1/8$	1958	3.597×10^{-7}	6.695	2.534×10^{-5}	5.421	0.002252	4.191
$1/16$	7366	4.648×10^{-9}	6.274	7.065×10^{-7}	5.165	0.0001344	4.067
$1/32$	28550	6.737×10^{-11}	6.108	2.116×10^{-8}	5.061	8.26×10^{-6}	4.024

Table 6.6: Errors and Rate of Convergence for the Full SQGE (2.28), Test 5

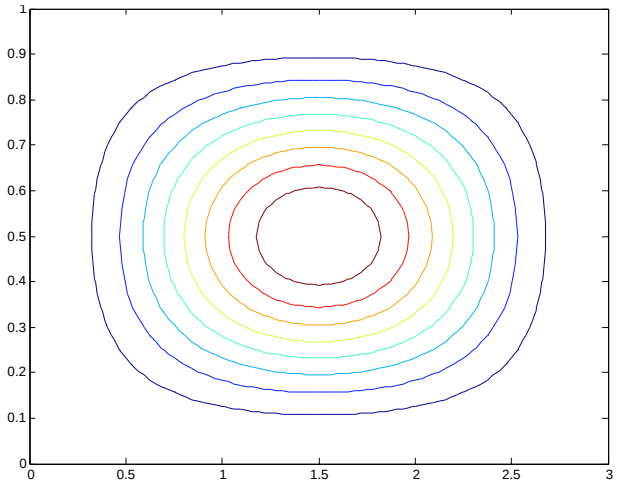

Figure 6.6: Full SQGE (2.28), Test 5: Streamlines of the approximation, ψ^h, $h = \frac{1}{32}$, and 28550 DoFs.

We note that the errors in Table 6.6 follow the theoretical rates of convergence predicted by the estimates (5.28) - (5.30) in Proposition 5.4. Again, since the exact solution (6.11) does not display any boundary layers, we see that the orders of convergence in Table 6.6 are close to the theoretical ones for the fine meshes, but are higher than expected for the for the coarse meshes.

Test 6: In this test, we take the same exact solution as used in *Test 4*, i.e.

$$\psi(x, y) = \left[\left(1 - \frac{x}{3}\right)\left(1 - e^{-20x}\right)\sin \pi y\right]^2. \tag{6.12}$$

The forcing term F and the homogeneous boundary conditions correspond to the exact solution (6.12).

Figure 6.7 presents the streamlines of the approximate solution obtained by using the Argyris Finite Element on a mesh with $h = \frac{1}{32}$ and 28550 DoFs. We note that the streamlines look as we expect and are similar to those given by Figure 10 in [39], which uses the same exact solution. Since the exact solution is

available, we can compute the errors in various norms. Table 6.7 presents the errors e_0, e_1, and e_2 (i.e., the L^2, H^1, and H^2 errors, respectively) for various values of the mesh sizes, h.

h	$DoFs$	e_0	L_2 order	e_1	H^1 order	e_2	H^2 order
$1/2$	170	0.3497	–	1.9	–	44.05	–
$1/4$	550	0.0302	3.533	0.4279	2.15	21.74	1.019
$1/8$	1958	0.001507	4.324	0.06085	2.814	5.661	1.941
$1/16$	7366	3.225×10^{-5}	5.547	0.004042	3.912	0.7379	2.94
$1/32$	28550	5.672×10^{-7}	5.829	0.000161	4.65	0.0597	3.628

Table 6.7: Errors and Rate of Convergence for the Full SQGE (2.28), Test 6

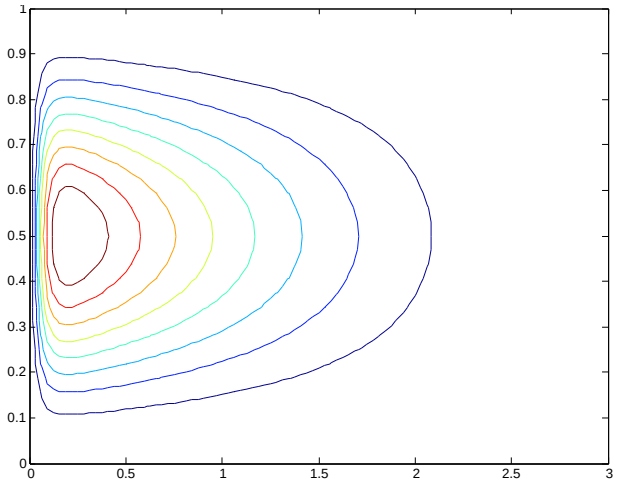

Figure 6.7: Full SQGE (2.28), Test 6: Streamlines of the approximation, ψ^h, $h = \frac{1}{32}$, and 28550 DoFs.

We note that the errors in Table 6.7 follow the theoretical rates of convergence predicted by the estimates (5.28) - (5.30) in Proposition 5.4. Again for an exact solution which has a western boundary layer, we see that the orders of convergence in Table 6.7 are close to the theoretical ones for the fine meshes, but not as close for the coarse meshes. We attribute this to the inaccuracies at the thin boundary layer on the left-hand side (i.e., at $x = 0$). The finer the mesh gets, the better this boundary layer is captured and the better the numerical accuracy becomes.

6.2 SQGE Two-Level

The main goal of this section is to verify the theoretical rates of convergence developed in Subsection 5.1.1 by comparing with the observed rates of convergence in our numerical tests. Unlike the previous section, for the two-level method we must demonstrate rates of convergence for two different meshes, the fine mesh, h, and the coarse mesh H. Since the error corresponding to the coarse mesh dominates the error corresponding to the fine mesh the rate of convergence in the coarse mesh is easy to demonstrate. To this end one need only pick a constant fine mesh and then refine the coarse mesh. By doing this one is able to demonstrate the rate of convergence in the coarse mesh. However, the rate of convergence in the fine mesh is a bit more trick to

demonstrate, because as stated previously the coarse mesh error dominates the fine mesh error and therefore one must balance the error between the fine mesh and the coarse mesh so as to be able to demonstrate the rate of convergence in the fine mesh. To this end we set the error terms in (5.56) equal to eachother to come up with the relationship

$$h = (\ln h)^{\frac{1}{8}} H^{\frac{5}{4}}. \tag{6.13}$$

This relation is super linear and essentially means that the coarse mesh H must be about half the size the fine mesh h.

To this end we apply the Two-Level method to the SQGE (2.28) with $Re = Ro = 1$ and exact solution

$$(\sin 4\pi x \cdot \sin 2\pi y)^2 . \tag{6.14}$$

Additionally, the homogeneous boundary conditions are $\psi = \dfrac{\partial \psi}{\partial \mathbf{n}} = 0$ and the forcing function F corresponds to applying the SQGE to the exact solution (6.14). Theses BCs and exact solution will be used in all the Two-Level tests that follow.

First, we benchmark our numerical tests by running SQGE without the two-level method. Comparing to this benchmark will allows us to compare errors in the H^2 norm for SQGE to the errors in H^2 norm with the two-level method applied.

h	$DoFs$	e_2	H^2 order	time (s)
$1/2$	70	174.5	–	0.70114
$1/4$	206	45.11	1.951	0.63921
$1/8$	694	9.286	2.28	3.3169
$1/16$	2534	0.6503	3.836	15.105
$1/32$	9670	0.03566	4.189	66.037
$1/64$	37766	0.002109	4.08	303.05

Table 6.8: Benchmark Errors and Rate of Convergence SQGE (2.28).

As can be seen in Table 6.8 the initial error is quite large in the H^2 norm. This is due to lack of resolution in the approximate solution because of the mesh coarseness. The given exact solution (6.14) has a period of $\dfrac{1}{2}$ in the x-direction and a period of one in the y-direction, therefore we must have a mesh size that much smaller than $\dfrac{1}{2}$ to be able to approximate the function appropriately. However, we see that by $h = \dfrac{1}{64}$ the error has on the order of 10^{-3} and the rate of convergence matches the theoretical rate of convergence predicted in Section 5.2.

H	$DoFs$ for H	h	$DoFs$ for h	e_2	H^2 order
$1/2$	70	$1/4$	206	45.44	–
$1/4$	206	$1/8$	694	10.89	2.061
$1/8$	694	$1/16$	2534	0.8404	3.696
$1/16$	2534	$1/32$	9670	0.04075	4.366
$1/32$	9670	$1/64$	37766	0.002141	4.25
$1/64$	37766	$1/128$	149254	0.0001298	4.044

Table 6.9: Errors and Rate of Convergence in h for the Two-Level method applied to SQGE (2.28).

In Table 6.9 we use the relationship (6.13) to determine a mesh size relationship between h and H. As stated previously, this relation implies that $H \approx \frac{h}{2}$ and therefore we chose the (H, h) pairs corresponding to

$$\left\{\left(\frac{1}{2}, \frac{1}{4}\right), \left(\frac{1}{4}, \frac{1}{8}\right), \left(\frac{1}{8}, \frac{1}{16}\right), \left(\frac{1}{16}, \frac{1}{32}\right), \left(\frac{1}{32}, \frac{1}{64}\right), \left(\frac{1}{64}, \frac{1}{128}\right)\right\}$$

so as to demonstrate the rate of convergence in h. As can be seen in Table 6.9 the rate of convergence does, in deed, approach the rate of convergence predicted in Subsection 5.1.1. Additionally, we see that the H^2 errors are of the same order as the corresponding errors in Table 6.8 for the same value of h.

To demonstrate the rate of convergence in H we take a constant fine mesh size of $h = \frac{1}{128}$ and vary the coarse mesh H. To this end we chose the (H, h) pairs corresponding to

$$\left\{\left(\frac{1}{2}, \frac{1}{128}\right), \left(\frac{1}{4}, \frac{1}{128}\right), \left(\frac{1}{8}, \frac{1}{128}\right), \left(\frac{1}{16}, \frac{1}{128}\right), \left(\frac{1}{32}, \frac{1}{128}\right), \left(\frac{1}{64}, \frac{1}{128}\right)\right\}.$$

H	$DoFs$ for H	h	$DoFs$ for h	e_2	H^2 order
$1/2$	70	$1/128$	149254	7.653	–
$1/4$	206	$1/128$	149254	5.916	0.3715
$1/8$	694	$1/128$	149254	0.5373	3.461
$1/16$	2534	$1/128$	149254	0.0199	4.755
$1/32$	9670	$1/128$	149254	0.0003779	5.719
$1/64$	37766	$1/128$	149254	1.381×10^{-5}	4.775

Table 6.10: Errors and Rate of Convergence in H for the Two-Level method applied to SQGE (2.28).

As can be seen in Table 6.10 the rate of convergence does, in deed, approach the rate of convergence predicted in Subsection 5.1.1. Additionally, we see that the H^2 errors are of the same order as the corresponding errors in Table 6.8 for the same value of h.

6.3 QGE

In this section we will present numerical tests to verify the theoretical error bounds derived in Section 5.2. The numerical tests will be very similar to those used in Subsection 6.1.3, except that the exact solution will have time dependence added to it. This will allow us to verify the rates of convergence in both the spatial domain and in the time domain.

6.4 LES

In this section we will present numerical tests to verify the theoretical error bounds derived in Section 5.3. Additionally, this section will be used to compare the results of the LES to DNS with the intention of demonstrating the appropriateness in the choice of closure model.

Chapter 7

Future Work

Below are the steps required to finish this thesis and a proposed deadline to finish each step.

- Stationary QGE $\surd$
  - Coding $\surd$
  - Error Analysis $\surd$
  - Two Level Method $\surd$
    - Coding $\surd$
    - Error Analysis $\surd$
- Time Dependent QGE
  - Coding - 01 June 2012
  - Error Analysis - 01 August 2012
  - Two Level Method
    - Coding - 15 August 2012
    - Error Analysis - 15 September 2012
- LES
  - Coding - 15 October 2012
  - Error Analysis - 01 February 2013
- Thesis Defense - April 2013

Table 7.1: Steps to finish thesis and proposed timeline.

Bibliography

[1] J. H. Argyris, I. Fried, and D. W. Scharpf. The TUBA family of plate elements for the matrix displacement method. *Aero. J.*, 72:701–709, 1968.

[2] V. Barcilon, P. Constantin, and E. S. Titi. Existence of solutions to the Stommel-Charney model of approximate deconvolution models of turbulence: Analysis, phenomenology and numerical analysis the Gulf Stream. *SIAM J. Math. Anal.*, 19(6):1355–1364, 1988.

[3] M. Bernadou. Straight and curved finite elements of class C^1 and some applications to thin shell problems. In *Finite element methods (Jyväskylä, 1993)*, volume 164 of *Lecture Notes in Pure and Appl. Math.*, pages 63–77. Dekker, New York, 1994.

[4] L. Berselli, T. Iliescu, and W. Layton. *Mathematics of large eddy simulation of turbulent flows.* Springer Verlag, 2006.

[5] D. Braess. *Finite elements: Theory, fast solvers, and applications in solid mechanics.* Cambridge University Press, 2001.

[6] J. M. Cascon, G. C. Garcia, and R. Rodriguez. A priori and a posteriori error analysis for a large-scale ocean circulation finite element model. *Comp. Meth. Appl. Mech. Eng.*, 192(51-52):5305–5327, 2003.

[7] M. E. Cayco and R. A. Nicholaides. Finite element technique for optimal pressure recovery from stream function formulation of viscous flows. *Math. of Comp.*, 46(174), 1986.

[8] P. G. Ciarlet. *The finite element method for elliptic problems.* North-Holland, 1978.

[9] P. F. Cummins. Inertial gyres in decaying and forced geostrophic turbulence. *J. Mar. Res.*, 50(4):545–566, 1992.

[10] B. Cushman-Roisin. *Introduction to geophysical fluid dynamics.* Prentice Hall, Englewood Cliffs, New Jersey, 1994.

[11] B. Cushman-Roisin and J. M. Beckers. *Introduction to geophysical fluid dynamics: Physical and numerical aspects.* International Geophysics. Elsevier Science & Technology, 2011.

[12] H. E. Dijkstra. *Nonlinear physical oceanography: A dynamical systems approach to the large scale ocean circulation and el Nino*, volume 28. Springer Verlag, 2005.

[13] H. E. Dijkstra. *Dynamical Oceanography.* Springer Verlag, 2008.

[14] V. Dominguez and F. J. Sayas. Algorithm 884: A simple Matlab implementation of the Argyris element. *ACM Transaction on Mathematical Software*, 35(2), 2008.

[15] F. Fairag. A two-level finite-element discretization of the stream function form of the Navier-Stokes equations. *Comp. Math. Applic.*, 36(2):117–127, 1998.

[16] F. Fairag. Numerical computations of viscous, incompressible flow problems using a two-level finite element method. *SIAM J. Sci. Comp.*, 24(6):1919–1929, 2003.

[17] G. J. Fix. Finite element models for ocean circulation problems. *SIAM J. on Appl. Math.*, 29(3):371–387, 1975.

[18] G. J. Fix, M. Gunzburger, R. Nicolaides, and J. Peterson. Mixed finite element approximations for the biharmonic equations. *Proc. 5th Internat. Sympos. on Finite Elements and Flow Problems (JT Oden, ed.), University of Texas, Austin*, pages 281–286, 1984.

[19] M. Ghil, M. D. Chekroun, and E. Simonnet. Climate dynamics and fluid mechanics: Natural variability and related uncertainties. *Physica D: NONLINEar Phenomena*, 237:2111–2126, 2008.

[20] V. Girault and P. A. Raviart. *Finite element approximation of the Navier-Stokes equations: Theory and algorithms*. Volume 749 of Lecture Notes in Mathematics. Springer-Verlag, 1979.

[21] V. Girault and P. A. Raviart. *Finite element methods for Navier-Stokes equations: theory and algorithms*, volume 5 of *Springer Series in Computational Mathematics*. Springer-Verlag, 1986.

[22] R. J. Greatbatch and B. T. Nadiga. Four-gyre circulation in a barotropic model with double-gyre wind forcing. *J. Phys. Oceanogr.*, 30:1461–1471, 200.

[23] M. D. Gunzburger. *Finite element methods for viscous incompressible flows*. Computer Science and Scientific Computing. Academic Press Inc, 1989. A Guide to Theory, Practice, and Algorithms.

[24] M. D. Gunzburger and J.S. Peterson. Finite-element methods for the streamfunction-vorticity equations: Boundary-condition treatments and multiply connected domains. *SIAM J. Sci. Stat. Comp.*, 9:650, 1988.

[25] M. D. Gunzburger and J.S. Peterson. On finite-element approximations of the streamfunction-vorticity and velocity-vorticity equations. *Internat. J. Numer. Meth. Fluids*, 8(10):1229–1240, 1988.

[26] T. Iliescu. *Large eddy simulation for turbulent flows*. PhD thesis, University of Pittsburgh, 2000.

[27] H. Ingstad and A. S. Instad. *The Viking discovery of America: The excavation of a Norse settlement in L'Anse aux Meadows, Newfoundland*. Breakwater Books, 2000.

[28] V. M. Ipatova, V. I. Agoshkov, G. M. Kobelkov, and V. B. Zalesny. Theory of solvability of boundary value problems and data assimilation problems for ocean dynamics equations. *Russ. J. Numer. Anal. Math. Modelling*, 25(6):511–534, 2010.

[29] C. Johnson. *Numerical solution of partial differential equations by the finite element method*, volume 32. Cambridge university press New York, 1987.

[30] W. Layton. A two-level discretization method for the Navier-Stokes equations. *Comp. Math. Applic.*, 26(2):33–38, 1993.

[31] W. J. Layton. *Introduction to the numerical analysis of incompressible viscous flows*, volume 6. Society for Industrial and Applied Mathematics (SIAM), 2008.

[32] C. LeProvost, C. Bernier, and E. Blayo. A comparison of two numerical methods for integrating a quasi-geostrophic multilayer model of ocean circulations: finite element and finite difference methods. *J. Comput. Phys.*, 110:341–359, 1994.

[33] A. J. Majda. *Introduction to PDEs and waves for the atmosphere and ocean*. AMS, New York, 2003.

[34] A. J. Majda and X. Wang. *Non-linear dynamics and statistical theories for basic geophysical flows*. Cambridge University Press, 2006.

[35] J. McWilliams. *Fundamentals of geophysical fluid dynamics*. Cambridge Univ Pr, 2006.

[36] T. T. Medjo. Mixed formulation of the two-layer quasi-geostrophic equations of the ocean. *SIAM J. on Appl. Math.*, 15(4):489–502, 1999.

[37] T. T. Medjo. Numerical simulations of a two-layer quasi-geostrophic equation of the ocean. *SIAM J. on Appl. Math.*, 37(6):2005–2022, 2000.

[38] N. A. Mörner. Earth rotation, ocean circulation and paleoclimate. *GeoJournal*, pages 419–430, 1995.

[39] P. G. Myers and A. J. Weaver. A diagnostic barotropic finite-element ocean circulation model. *J. Atmos. Oceanic Technol.*, 12:511, 1995.

[40] Masayuki Okabe. Full-explicit interpolation formulas for the Argyris triangle. *Comp. Meth. in Appl. Mech. and Eng.*, 106:381–394, 1993.

[41] J. Pedlosky. *Geophysical fluid dynamics*. Springer, second edition, 1992.

[42] J. Roach. Artic melt opens Northwest Passage. `http://news.nationalgeographic.com/news/2007/09/070917-northwest-passage.html`, September 2007.

[43] O. San, A. E. Staples, Z. Wang, and T. Iliescu. Approximate deconvolution large eddy simulation of a barotropic ocean circulation model. *Ocean Model.*, 2011. Submitted.

[44] O. San, A. E. Staples, Z. Wang, and T. Iliescu. Approximate deconvolution large eddy simulation of a stratified two-layer quasigeostrophic ocean model. *Ocean Model.*, 2011. Submitted.

[45] X. Shao and D. Han. A two-grid algorithm based on newton iteration for the stream function form of the Navier-Stokes equations. *Appl. Math. J. Chinese Univ.*, 26(3):368–378, 2011.

[46] G. Siedler, J. Church, and J. Gould. *Ocean circulation and climate: Observing and modelling the global ocean*, volume 77. Academic Press, 2001.

[47] W. N. R. Stevens. Finite element, stream function-vorticity solution of steady laminar natural convection. *Int. J. Num. Meth. Fluids*, 2:381–394, 1982.

[48] G. K. Vallis. *Atmosphere and ocean fluid dynamics: Fundamentals and large-scale circulation*. Cambridge University Press, 2006.

[49] J. Wang and G. K. Vallis. Emergence of Fofonoff states in inviscid and viscous ocean circulation models. *J. Mar. Res.*, 52:83–127, 1994.

[50] G. Wolansky. Existence, uniqueness and stability of stationary barotropic flow with forcing and dissipation. *Comm. Pure Appl. Math.*, 41:19–46, 1988.

[51] J. Xu. A novel two-grid method for semilinear elliptic equations. *SIAM J. on Sci. Comp.*, 15(1):231–237, 1994.